

Design and production of a scaled floating substructure

Floating Wind University Challenge

Daan Koetzier

Sebastiaan van Putten

Sowmya Iyer

Carlos Pérez Moreno



Design and production of a scaled floating substructure

by

Daan Koetzier
Sebastiaan van Putten
Sowmya Iyer
Carlos Pérez Moreno

Institution:	Delft University of Technology Denmark Technical University
Place:	Norwegian University of Science and Technology Faculty of Aerospace Engineering, TU Delft Department of Wind Energy, DTU Department of Marine Technology, NTNU
Project Duration:	Jan, 2022 - May, 2022

Cover Image: NOV: Tri-Floater Floating Offshore Wind Turbine Foundation
<https://www.nov.com/products/tri-floater-floating-offshore-wind-turbine-foundation>

Contents

1	Introduction	1
1.1	Floating wind energy. A new technology	1
1.2	Brief history of Floating Wind.	2
1.3	Project overview	2
1.4	Challenges of floating wind energy	4
1.4.1	Technical challenges	4
1.4.2	Socio-Economic Challenges	5
1.4.3	Codes, meshes and models.	5
2	Design Choices	6
2.1	Available concepts in the market	6
2.1.1	Spar	6
2.1.2	Tension-Leg Platform.	6
2.1.3	Barge	6
2.1.4	Semi-submersible	7
2.2	Choice of concept for Competition Specifications.	7
3	Hydrostatic and Hydrodynamic Modelling	9
3.1	Hydrostatic analysis	9
3.2	Hydrodynamic Simulation	9
3.2.1	Model structure	10
3.2.2	Inclination angle.	15
3.3	Potential theory. NEMOH	15
3.4	Simulation results	18
3.4.1	Natural frequency analysis.	18
3.4.2	Full simulations	21
3.5	Simulation challenges and pitfalls	22
4	Production of the scaled model	24
4.1	Model Design	24
4.2	Bill of Materials	25
4.3	Production Plan	26
4.3.1	Pre-production stage	26
4.3.2	Production stage	26
4.4	Structural integrity	28
4.5	Practicality of construction.	29
5	Testing of the model	30
5.1	Wind Tunnel Test	30
5.2	Power generation efficiency	33
5.3	Water Test of Model.	34
6	Scalability for further production	36
6.1	Design & Production Choices For a Full-Scale Floater.	36
6.2	Cost Efficiency At Full-Scale.	37

7 Conclusion	39
7.1 Future Improvements	39
7.2 Acknowledgements	39
References	40

1

Introduction

1.1. Floating wind energy. A new technology

Our planet has maintained a relatively stable temperature over the last few thousands of years, but this has changed since the advent of the industrial age [1]. The emission of greenhouse gases that remain trapped in our atmosphere has been steadily increasing the average temperature of the earth at an alarming rate [2], leading to a growing rise in the global temperature. Figure 1.1 shows the almost 1° increase in temperature above the average over just the last 20 years as compared to the relatively steady temperature of -0.5° below the average over the last 150 years. This shows that within less than 200 years, we have seen an increase in the global temperature of over 1° , most of which has occurred within the last 30 years.

At the current rate of warming, we are on the path to devastating results, with a warming of up to 4° by 2100 [2]. The energy industry contributes to a large percentage of the greenhouse gas emissions, with coal accounting for 40% of the growth of carbon dioxide emissions in 2021 [4]. The jump in fossil fuels is pushing the greenhouse gas emissions to a new peak [4], which is dangerous and will lead to detrimental effects on the natural environment and wildlife [2]. The need to transition to emission-free renewable energy sources could not be more urgent and necessary, and this means that the amount of electricity produced from renewables needs to grow to 86% by 2050 [5]. To achieve this transition, the amount of energy produced from wind needs to grow.

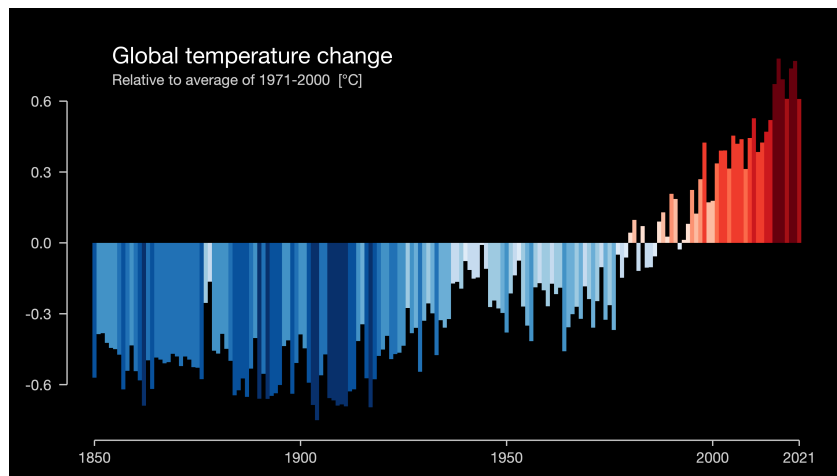


Figure 1.1: Global Temperature Change. Reprinted from [3]

The high wind resource far from the coast and the large areas of available space make it a very attractive location for wind turbines, but the deep seabeds above 50-60 m make it difficult or impossible to have bottom fixed structures. With this comes the need for floating wind energy.

Floating wind energy, although still under research and development phase, is drawing more attention at every step that is taken.

Historically, the floating wind energy projects have been developed based on existing oil and gas industry technologies, with high safety margins compare to those of general wind energy. Therefore, costs are significantly high and the market expansion relatively low compared to bottom-fixed offshore technologies. Therefore, one of the challenges is to develop safe but scalable floating designs that can be introduced quickly in the market, allowing a quick energy transition, as demanded by the last IPCC report.

1.2. Brief history of Floating Wind

The history of floating wind energy can be told briefly.

On 2009, the BlueH Tension-Leg Platform (TLP) was deployed in souther Italy as a scale prototype. It was decommissioned however few months later.

In 2010, the Hywind demo was installed north of Stavanger, Norway, becoming the first full-scale floating wind turbine [6]. It is a 2.3MW Siemens Wind Turbine, mounted on a 100-meter draught SPAR system.

The following year, WindFloat prototype was installed off the Portuguese coast. This is a semi-submersible type, based on three legs with heave plates, whose stability is based on a large water-plane area. The effect of the heave plates is to reduce the heave natural frequency, so that no resonance is produced due to wave excitation, and the heave response to wave loads is damped.

On the same year, the Japanese project named FORWARD started, leading to the installation of a 2MW Wind Turbine on a semi-submersible structure connected to the grid in 2013. The substation was installed using a SPAR-type substructure. This project has continued with its phase II, consisting on the installation of a 5 and a 7MW Wind Turbines on different semi-submersible structures. More information can be found on <http://www.fukushima-forward.jp/english/>.

1.3. Project overview

Firstly, the type of floater for the project was determined based on a preliminary qualitative analysis of the conventional floater types available in the market. These were assessed based on the wind and wave conditions as well as the seabed depth, and the semi-submersible floater seems to be the best choice. Details on the criteria of each floater can be found in Chapter 2.

During the initial planning of the project timeline in January, a Gantt chart was made and can be seen in Figure 1.2. However, as it is often the case in many engineering projects, we were not able to stick to the timeline and many things were delayed. For instance, the floater and mooring analysis were delayed, as explained in Section 3.5.

There was an initial work plan as shown in the abstract, that for many reasons was changed along the way. Firstly, the initial plan to use SolidWorks and the BEM Rosetta interface proved to be an issue due to the meshing. Only much later in the process were we able to successfully use Salome to generate the mesh to run in NEMOH, thereby delaying the floater assessment portion greatly. Furthermore, the analytical analysis of the mooring lines in MoorDyn also took longer than expected because of the difficulty in configuration due to the definition of the initial conditions. Additionally, the booking of the OJF for the wind tunnel test of the turbine could only be done in late March, which also delayed the aerodynamic force inputs to

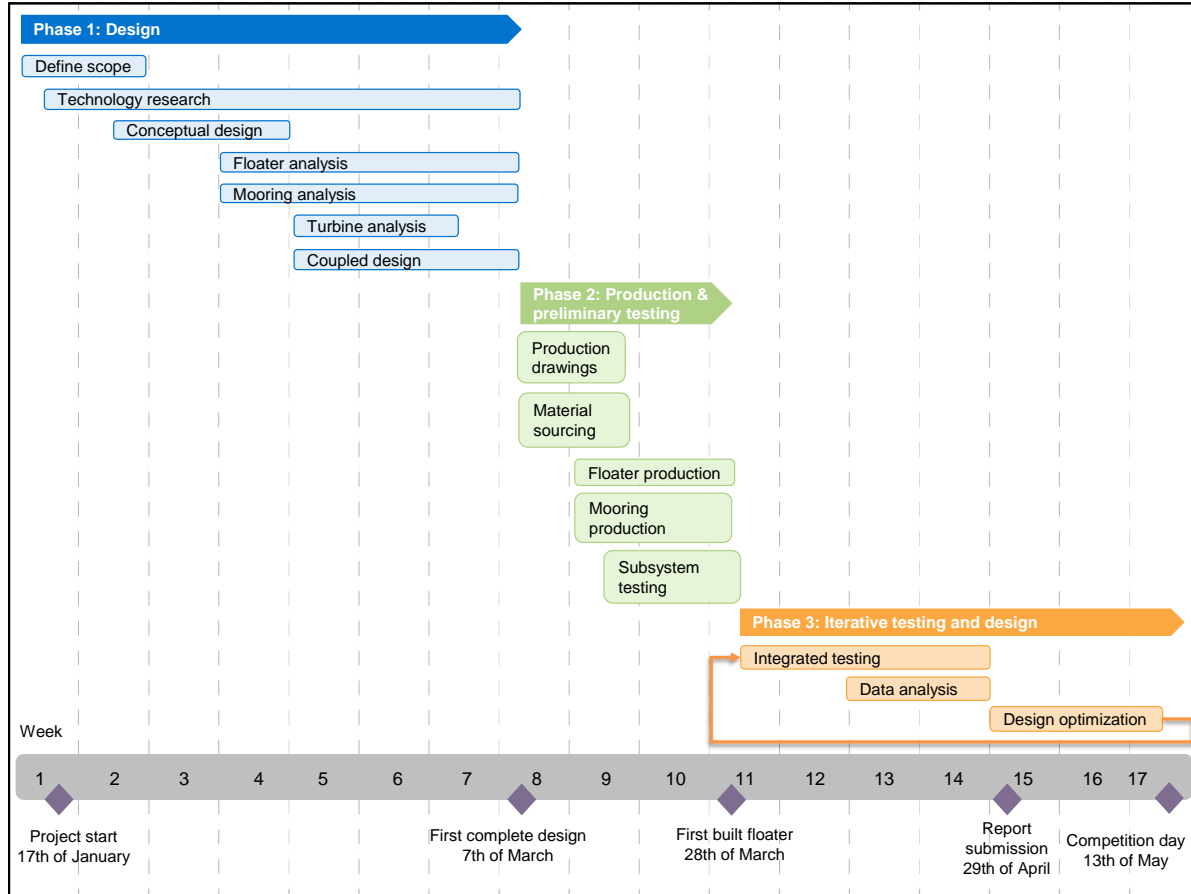


Figure 1.2: Original Gantt Chart

the equations of motions. Lastly, the four of us had exams from the 1st of April till the 25th of April, which unfortunately halted the work plan and further delayed our ability to progress.

The updated overview of the project is seen in Figure 1.3, which describes the final work flow that was followed and implemented for the dynamic analysis of the floating structure.

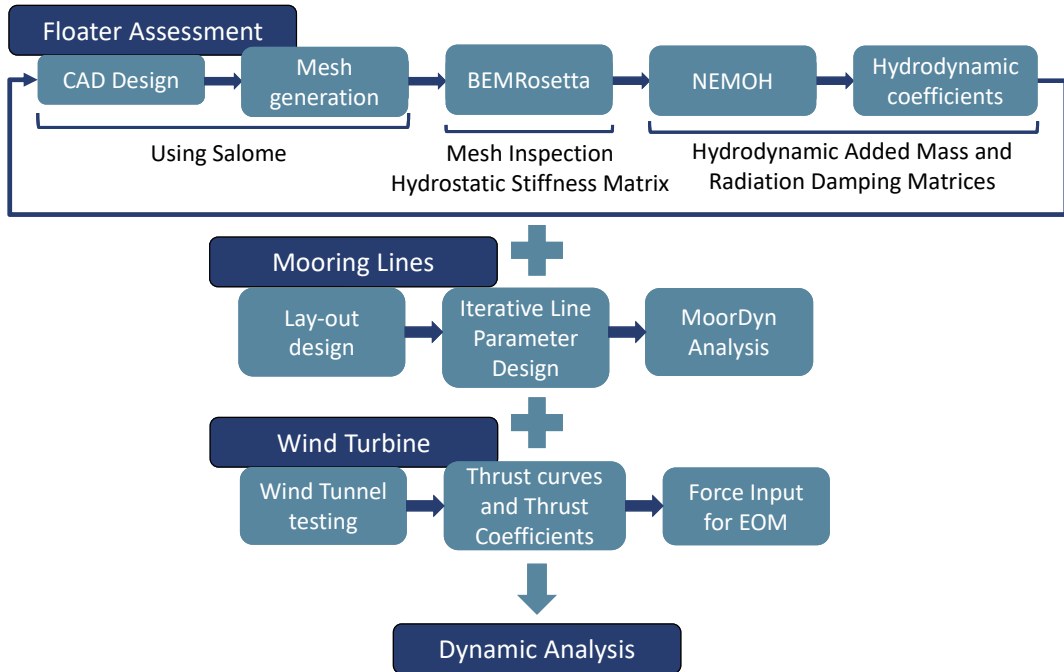


Figure 1.3: Updated Project Overview

The dynamic analysis was done iteratively to take into account the natural frequencies of the floater to ensure that they fall out of the range of the JONSWAP spectrum, and that the length of the arms and diameters of the spars provide enough buoyancy and water-plane area for stability while remaining easy to manufacture. The details of the analysis are described in detail in Chapter 3.

Based on the results of the simulation, the dimensions of the various parts for the floater were modified and brackets to connect the spars and heave plates were designed and 3D printed, detailed in Chapter 4. The details on the aerodynamic testing of the turbine, an analysis of the effects of wind and wave coupling as well as water tests of the 3D printed parts can be found in Chapter 5.

Lastly, the scalability of our model is addressed, taking into account production costs, building, transportation and installation of the floater.

1.4. Challenges of floating wind energy

Every new technology faces significant challenges and difficulties in its development at first, and this is clearly the case of floating wind energy. The challenges can be classified in technical, scalability and socio-economical challenges. Scalability challenges will be addressed in Chapter 6.

1.4.1. Technical challenges

As it will be explored throughout the report, technical challenges are the primary obstacle in the deployment of large floating wind farms. The main issue encountered is the unsteadiness of the system. As compared to offshore bottom-fixed, the displacements of the system are much more significant, and are directly coupled with the loads experienced by the Wind Turbine Generator (WTG) via unsteady aerodynamics. Additionally the controller will play a major role in both balancing inclination motions, and optimising the energy harvesting of the system, while limiting the loads. This intrinsic characteristic of the floating wind energy leads to the

need of developing hydro-servo-aeroelastic tools capable of accurately simulating the wave-wind conditions faced in order to perform optimisations of the designs.

The wave loading plays a major role in floating structures. In general it has been found that most simulations are based on linear waves, but for the conditions far offshore highly nonlinear waves are encountered, thus the load analysis should take into account a larger range of external forces, of both waves and wind, as compared to near-shore and onshore wind turbines.

Currently, traditional turbines are build for an onshore environment, and scaled to be placed offshore. More advanced scaling measures are implemented to move turbines offshore, including redesigning blades with airfoils meant for higher Reynolds number applications, and increasing the laminate of the blades for a higher stiffness. However, these design changes still rely on the fundamental design of a fixed turbine that is not subjected to highly unsteady motions of the base. To really develop floating offshore wind energy, the whole system design would need to be remodelled, to take into account the fact that the turbines will undergo heaving and pitching motions strongly coupled with the unsteady aerodynamic loads. The design should ideally be integrated with the weight distribution of the individual components, because their relative position will affect the centre of gravity of the turbine and hence, the required restoring moment of the floater.

Additionally, the turbines are situated further offshore, which leads to the need for substations as well as extremely long and expensive cabling to bring the energy back to the consumers. These long cables result in large power losses as they have to travel many kilometres to reach the substations. Furthermore, the turbines are no longer standing still as they do for onshore or bottom fixed structures and hence, the cabling also needs to take into account the movement with the turbine and the loads on the cable as it moves. This area is still early in its research stage and as of now, there are no concrete solutions to the issue of cabling and power losses.

1.4.2. Socio-Economic Challenges

Wind energy faces generally a large opposition from citizens that are affected by it in different ways, such as visually or acoustically. One of the advantages in this aspect of floating wind energy is the ability to be deployed far from the coast, reducing these impacts on people. It will however, still have an impact, as onshore substations are needed during the operation, and large coastal spaces might be used during commissioning and decommissioning phases. This aspect should be addressed with transparency and involvement of the local governments, developers and manufacturers to ensure the projects can be developed and the energy transition accelerated.

From a biodiversity point of view, it is important that studies are conducted on the development of aquatic life surrounding the Floating Offshore Wind Farms (FOWF), and the impact of mooring lines, cables and the WTG system on the existing habitats. The effect on offshore ornithology as well as shellfish at the base of the seabed as well as those that grow on the structures and hence will need to be relocated during decommissioning also needs to be taken into account.

Economically, as it will be addressed in Chapter 6, the necessity of establishing the supply chain

1.4.3. Codes, meshes and models

Examples of meshes, CAD models, codes and simulation results will be publicly available and can be found on: <https://github.com/carlospmo/FloatingWind>.

2

Design Choices

One of the first issues to address is the floater design choice. Several concepts are under study and already implemented in test facilities, or under real conditions. These concepts are analysed in Section 2.1. Then, it is important to consider the location-specific characteristics in order to choose the most suited design. This is discussed in Section 2.2. Finally, after adopting a single concept, different designs are evaluated and simulations are performed, shown in Section 3.2. These simulations are the basis of further detailed floater design.

2.1. Available concepts in the market

The available concepts in the market will be briefly explained in this section, detailing how each concept achieves its stability and the complexity of the mooring lines.

2.1.1. Spar

In a spar structure, the system is stabilised by means of a counterweight (ballast), requiring a small water-plane area. The structure is very simple, as most designs consist of a vertical cylinder with heave plates attached. The spar achieves its stability by having the centre of gravity below the buoyancy centre, thereby creating a restoring moment when tilted. However, the depth of the seabed needs to be relatively high for the spar to be long enough to be effective. Furthermore, spars are generally moored using catenary lines, which have a large footprint.

2.1.2. Tension-Leg Platform

In the Tension-Leg Platform, the system is stabilised through the tension legs, requiring a very small water-plane area. This however leads to a difficult transport and installation, as the it is not stable by itself until the mooring system is not deployed. Although it has a small footprint, the fatigue on the taught mooring lines is a large issue that has not been fully researched into yet and hence, it is not the most preferred choice. Furthermore, the mooring creates a vertical tension on the cables and hence requires more expensive anchors to hold them in place. Therefore, generally a hybrid configuration is preferred.

2.1.3. Barge

A barge gets its stability from a large water-plane area. This leads to them having a large footprint on the water, and an even larger one at the seabed since they are usually moored with catenary lines. Although they are easy to assemble onshore and tow to the location, the size of the barge needed to withstand the wave height for the model would require it to be around the scale of a semi-sub.

2.1.4. Semi-submersible

A semi-sub gets its stability from its water-plane area and is moored with catenary lines and hence, has a very large footprint. It is stable on its own and can be assembled onshore and towed to sea for easy installation. The semi-sub is generally made of 3 to 4 spars that are connected together to provide stability and a larger area for buoyancy, but using less material. However, semi-subs are very sensitive to heave and hence, generally require additional heave plates at the bottom of the spars to damp the motion. Furthermore, as with all floaters that have catenary mooring, the horizontal motions are high, especially of surge since it is generally in the direction of the incoming wind and waves.

2.2. Choice of concept for Competition Specifications

A choice must be made for what general floater design will be chosen for further evaluation. For this, a weighted-criteria analysis can be carried out. By determining certain properties and attaching a relative importance value to these, a design can be found that best suits the contest requirements. The four floater types mentioned in Section 2.1 will be evaluated for the competition specific conditions based on the following criteria:

- Static and dynamic stability
- Response to incoming wave and wind direction
- Seabed type and mooring feasibility
- Construction feasibility
- Scalability

The competition requirements set a water depth of 90cm, a sandy seabed of 40cm depth that is prone to scour and a 20cm significant wave height. It also specifies that the hub height should be 70cm above the water. This requires the turbine to be raised by 30cm since the tower is 40cm high.

Spars require a water depth of around 100-150 m [7] and hence, the water depth of the competition may not be enough to achieve static stability. Furthermore, spars have the largest draft of all the floater types and hence, for such a shallow water depth and high significant wave height of about half the tower height, the response of the system may not have enough damping, leading to possibly large heaving and pitching motions and hence, the design would not be a viable choice.

TLPs are statically stable once the mooring lines are attached, but this is complicated to install on site. Although they have a low draft [7], the wave conditions will make the loads in the taught mooring lines build up rather quickly, leading to a large fatigue. In full scale conditions, TLPs are generally suited for more calm environments, since any force on the turbine would be transferred as a force on the mooring cables.

Barges have the lowest draft [7] and are very easy to install since they are statically stable on their own and can therefore be towed. However, the high significant wave height would require the barge to be around the scale of a semi-sub to have a large enough water-plane area to have a large enough restoring moment. Although it is easy to construct, the additional infill material makes it very heavy, making it less desirable, especially when up-scaling it to a full sized floater.

A semi-sub gives us the benefits of the spars and the barge, by achieving the stability from a larger water-plane area while reducing the amount of material used. It is also relatively easy to construct since it consists of many spars, that are essentially just pillars. The semi-sub draft is similar to that of a barge, though slightly higher due to space in between the spars, making it more prone to heave. Hence, with the addition of heave plates, it is statically and dynamically

the easiest option to make stable for the wind and wave conditions. The installation of a semi-sub is also easy, since the structure can be towed to the location and then moored using catenary lines, that take horizontal loads at the seabed and hence, require cheaper anchors. Finally, the design of the semi-sub is feasible to scale, since the adjustments of the loads and movement of the degrees of freedom at full scale are easy to account for by changing the distance between the spars to adjust the water-plane area or changing the length of the spars for buoyancy and weight. Hence, the semi-sub was the chosen floater for this contest.

3

Hydrostatic and Hydrodynamic Modelling

3.1. Hydrostatic analysis

The first requirement is to ensure static floating behaviour, that is, that the sum of vertical forces is zero:

$$\sum F_z = F_B - F_W = 0 \quad (3.1)$$

where F_B is the buoyancy force, and F_W is the weight of the system. This leads to the following equation:

$$l_{\text{submerged}} = \frac{m_{\text{total}}}{\rho A_{\text{waterplane}}} \quad (3.2)$$

For a buoy diameter of 0.1 m, a submerged length of 0.092 m is found. This means that the floater buoys need to be at least this long to stay afloat. The submerged length will increase if the mooring loads are applied.

3.2. Hydrodynamic Simulation

The dynamics of the floater-turbine system have a large influence on power production. The floater motions should be limited in order to achieve a maximum power generation efficiency. There are many ways to model the system. A fully integrated time-domain aerodynamic, hydrodynamic and mooring model could be used, such as FAST. The team opted to not pursue this type of simulation, since there was no previous experience and the available time was limited. An easier option would be frequency-domain analysis. It is possible to determine response amplitude operators (RAOs) of the system to analyse its frequency response, based on the frequency of the excitation forces. However, the system was deemed too complex to model only in frequency domain.

Instead, it was chosen to make a 3 degree of freedom dynamic model in MATLAB which solves the equations of motion of the system with an ODE4-solver (4th order Runge-Kutta method), to obtain the motions of the system in surge, heave and pitch. These are determined as the most important degrees of freedom. Since there was previous experience in the team with this type of model for a 2 degree of freedom spar floater, it was opted to take this model as a basis for the simulation of the semi-sub.

NEMOH was used to do a hydrodynamic analysis on the floater design and find the system matrices. The floater was initially designed using SolidWorks, and BEM Rosetta was used to convert the mesh to the required file for NEMOH to process to get the hydrodynamic matrices.

However, due to some mesh handling issues, the floater was redesigned in Salome and input directly to NEMOH. The outputs from NEMOH were checked by comparing them to analytical computations of the system matrices.

3.2.1. Model structure

To make the model, the equations of motion of the system must be obtained. These are found in the form of an analytically calculated mass matrix, and an added mass matrix, a damping matrix and a stiffness matrix found through NEMOH. The mass matrix is found as follows:

$$\mathbf{M} = \begin{bmatrix} m & 0 & mz_g \\ 0 & m & 0 \\ mz_g & 0 & I_{system} \end{bmatrix} \quad (3.3)$$

The masses of the system are found by weighing the turbine parts and estimating the floater weight, and the inertia and center of masses of the system are calculated analytically with help of the following diagram:

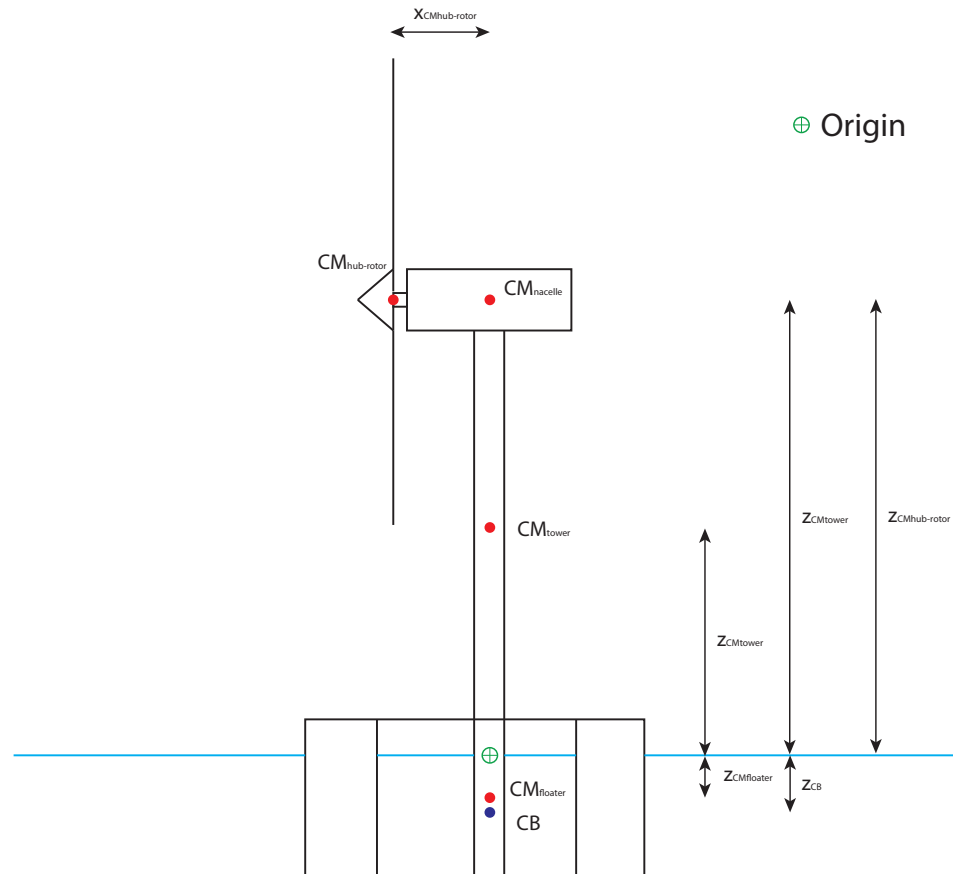


Figure 3.1: Center of masses in the turbine that are relevant for the moment of inertia of the system

Next, the hydrodynamic and aerodynamic loads on the structure must be determined. The hydrostatic and hydrodynamic loads are calculated by generating a wave climate using the given JONSWAP-spectrum and applying linear wave theory and Morisons equation. The

aerodynamic loads are determined through wind tunnel testing of the given turbine. The mooring of the system is modelled with MoorDyn, an open-source dynamic mooring line model. It uses a lumped-mass formulation for modelling axial elasticity, hydrodynamics, and seabed contact. The equations of motion are solved numerically with the ODE4-solver to obtain the floater displacements in the selected degrees of freedom.

Equations of motion

The equations of motion are found through a force balance that is a result of Newtons second law. The equations of motion are linearized for the sake of simplicity. This is not a really valid solution since displacements will be large, but the aim of the model is to make an approximation of the motion and not an exact solution. The general equation of motion of the system can be written as:

$$(\mathbf{M} + \mathbf{A}) \begin{bmatrix} \ddot{x}_1 \\ \ddot{x}_2 \\ \ddot{x}_3 \end{bmatrix} + \mathbf{B} \begin{bmatrix} \dot{x}_1 \\ \dot{x}_2 \\ \dot{x}_3 \end{bmatrix} + \mathbf{C} \begin{bmatrix} x_1 \\ x_2 \\ x_3 \end{bmatrix} = \begin{bmatrix} F_1 \\ F_2 \\ F_3 \end{bmatrix} \quad (3.4)$$

Where x_1 represents surge, x_2 represents heave and x_3 represents pitch. F_1 represents the forcing in surge direction, F_2 represents the forcing in heave direction and F_3 represents the moment in pitch direction. The mass matrix \mathbf{M} represents a matrix of the mass or inertia for the specific degree of freedom, the added mass matrix \mathbf{A} represents the added mass of the body due to the acceleration of the displaced water, the damping matrix \mathbf{B} represents hydrodynamic damping and the stiffness matrix \mathbf{C} represents the hydrostatic stiffness.

Computational matrix formulation

AxiMesh was used to generate a symmetrical spar in NEMOH. The range of wave frequency of 3 to 5 rad/s in steps of 0.1 rad/s were given as in input, and the damping matrix outputs were taken at 4.1 rad/s in accordance with the peak frequency of the JONSWAP-spectrum. NEMOH gives the output of the mass base on the displacement of water, inertia which is estimated assuming mass is distributed on the wetted surface, the hydrostatic stiffness matrices and the coordinates of the buoyancy centres. This output file was then processed using BEM Rosetta to calculate the stiffness matrix, the added mass matrix at infinite frequency and the damping matrix at 4.1 rad/s. The simulation was run for all degrees of freedom, but the final floater was reduced to the 3DOF system based on the prevalent wind and wave directions for the test. This was done as an initial estimate since the BEM Rosetta mesh had some issues, but later, the full floater was designed in Salome and run directly through NEMOH. This is detailed in Section 3.3. The outputs of NEMOH from the Salome version are of the same format as from AxiMesh, so the calculation of the loads was just updated with the new matrices to have a more accurate simulation result.

Hydrodynamic and -static loads

The hydrodynamic loads in surge and pitch are determined through Morisons equation, which describes the loads of a flow of water on tubular members. First, the JONSWAP spectrum is transferred to a time-domain wave field, using a range of frequencies and an Inverse Fast Fourier Transform of the spectrum. This is done by generating the wave amplitudes from the JONSWAP spectrum,

$$a_i = \sqrt{2 \cdot S_{JS}(\omega) \cdot \Delta\omega} \quad (3.5)$$

after which the wave field is generated using linear wave theory and an IFFT, where the waves are given a random set of phases ε_i :

$$\eta = a_i \cos(\omega_i t - k_i x + \varepsilon_i) \quad (3.6)$$

The wave velocities and accelerations are calculated as follows:

$$\begin{aligned} u &= a_i \omega_i \frac{\cosh k_i(z+h)}{\sinh kh} \cos(\omega t - k_i x + \varepsilon_i) \\ \frac{\partial u}{\partial t} &= -a_i \omega_i^2 \frac{\cosh k_i(z+h)}{\sinh kh} \cos(\omega t - k_i x + \varepsilon_i) \\ w &= -a_i \omega_i \frac{\sinh k_i(z+h)}{\sinh k_i h} \sin(\omega t - k_i x + \varepsilon_i) \\ \frac{\partial w}{\partial t} &= -a_i \omega_i^2 \frac{\sinh k_i(z+h)}{\sinh k_i h} \cos(\omega t - k_i x + \varepsilon_i) \\ \phi &= -\frac{a_i \omega_i}{k_i} \frac{\cosh k_i(z+h)}{\sinh kh} \sin(\omega t - k_i x + \varepsilon_i) \end{aligned} \quad (3.7)$$

The wave properties are found for a range of frequencies, and to find the final wave properties, these are superimposed by summing them. The wave properties are calculated at different positions, at $x = r_{Buoy}$, and at the second and third buoy, at $x = -r_{Buoy} \cos 60$. The wave climate looks as follows:

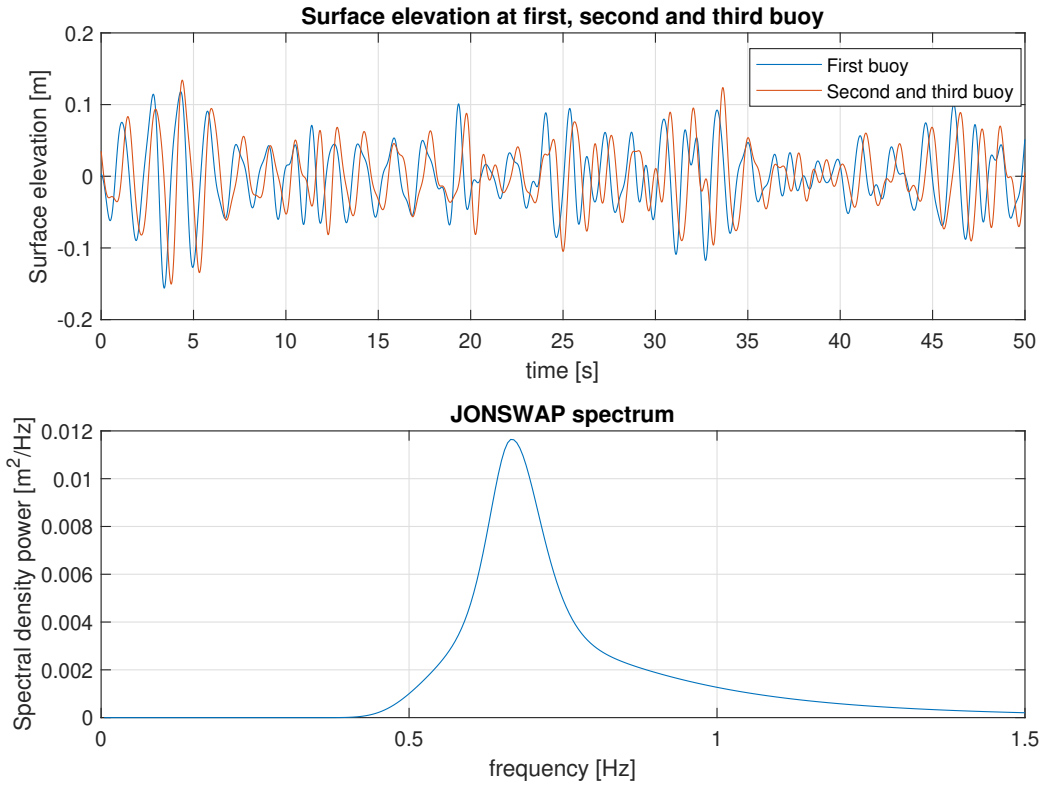


Figure 3.2: Wave climate and JONSWAP spectrum for $H_s = 0.2m$ and $T_p = 1.5s$

The wave properties are also found for a range of vertical coordinates z . They are computed for 100 points from the sea floor to mean water level, $[-0.9, 0]$. Wheeler stretching is not applied for the sake of simplicity. To find the force on the front buoy in surge, Morisons equation is applied over the submerged length of the floater. To find the full magnitude of the force,

the force distribution is integrated. The range of integration is from the bottom of the buoy to mean water level. The bottom of the buoy is dependent on the floaters heave and pitch, so this is calculated for every simulation timestep. This yields a new range of z-coordinates every timestep, and the relevant wave properties are found by interpolating from the initial z-coordinates used to determine the wave climate. Note that the drag force takes into account the relative velocity of the water to the floater, while for the inertia part only the water acceleration and not the floater acceleration is used. This is because this is already taken into account with the added mass matrix.

$$F_{1,\text{buoy}1} = \int_{z_{\text{bot}}}^0 \left[\rho A C_M \frac{\partial u}{\partial t} + \frac{1}{2} \rho D C_D (u - \dot{x}_1 - zx_3) |u - \dot{x}_1 - zx_3| \right] dz \quad (3.8)$$

This force is calculated for each buoy. The two buoys at the back of the floater use a different wave climate, which takes into account the distance between the buoys. The full force in surge is found by summing the force on the buoys and the middle tubular member. The inertia and drag coefficient used are $C_M = 2$ and $C_D = 0.6$.

To determine the force in heave, the dynamic and static pressure on the buoys is determined and summed with the inertia of the displaced water and the drag forcing:

$$F_{2,\text{buoy}1} = -\rho \phi A + \rho g A \eta + \rho C_{m_z} \nabla_s \dot{w} + \frac{1}{2} \rho A C_{D_z} (w - \dot{z}) |w - \dot{z}| \quad (3.9)$$

The first term in the equation is the dynamic pressure, and the second term the static pressure coming from the surface elevation of an incoming wave. The third term is the inertia component, where $C_{m_z} = 0.64$ and ∇_s is half the volume of a sphere with diameter D . Again, note that only the vertical wave acceleration and not the floater acceleration is taken into account for the inertia component, since this is included in the added mass matrix. The last term is the drag on the cylinder, which is calculated from the relative velocity of the water, where $C_{D_z} = 0.8$. The force on the other buoys and middle tube is determined in the same manner but with the different wave climate, and they are summed to find the total force.

To determine the moment in pitch from the horizontal wave velocity, the force is multiplied by its arm and integrated in a similar manner:

$$F_{3,\text{buoy}1} = \int_{z_{\text{bot}}}^0 \left[\rho \frac{\pi}{4} D^2 C_M \frac{\partial u}{\partial t} + \frac{1}{2} \rho D C_D (u - \dot{x}_1 - zx_3) |u - \dot{x}_1 - zx_3| \right] zdz \quad (3.10)$$

The total moment resulting from horizontal wave velocity is found by summing the resulting components from the three buoys and the middle tube, since all of them work in the same direction:

$$F_{3,\text{hor}} = F_{3,\text{buoy}1} + F_{3,\text{buoy}2} + F_{3,\text{buoy}3} + F_{3,\text{tube}} \quad (3.11)$$

The moment in pitch resulting from the force in heave direction is found by multiplying the different forces by their arms and summing:

$$F_{3,\text{vert}} = F_{2,\text{buoy}1} r_{\text{buoy}} - F_{2,\text{buoy}2} r_{\text{buoy}} \cos(60) - F_{2,\text{buoy}3} r_{\text{buoy}} \cos(60) \quad (3.12)$$

The total hydrodynamic moment in pitch is found as:

$$F_3 = F_{3,\text{hor}} + F_{3,\text{vert}} \quad (3.13)$$

Aerodynamic loads

The aerodynamic loads on the turbine are calculated through interpolation of the wind tunnel data, with the wind speed found at hub height. A constant environmental wind speed of 7.9 m/s is assumed, since this is the highest number in the given Beaufort range. To find the relative wind speed on the rotor, the turbine motion is taken into account as follows:

$$V_{rel} = V_{wind} - \dot{x}_1 - h_{hub}\dot{x}_3 \quad (3.14)$$

To determine the hub height h_{hub} , the model also takes into account the heave of the floater. The relative wind speed V_{rel} is used to determine the aerodynamic force on the rotor. The aerodynamic moment is calculated by multiplying the aerodynamic force by its moment arm, which is also dependent on heave.

Mooring

Semi-subs are usually moored using catenary lines. This type of mooring achieves its stability through the weight of the chains. The loads on the anchors from catenary mooring lines are horizontal and hence, the anchors needed are less expensive. However, to achieve stability, enough weight is needed and hence, long and heavy chains need to be used, which adds to the material cost and increases the footprint.

MoorDyn is used to simulate the mooring lines and their reaction forces. The line properties are specified in the program, and the dynamic mooring line behaviour is simulated parallel to the solving of the equations of motion. New positions of the floater are inputted into MoorDyn for every timestep, resulting in realistic mooring line behaviour. The mooring line shape for a small displacement is shown in figure 3.3.

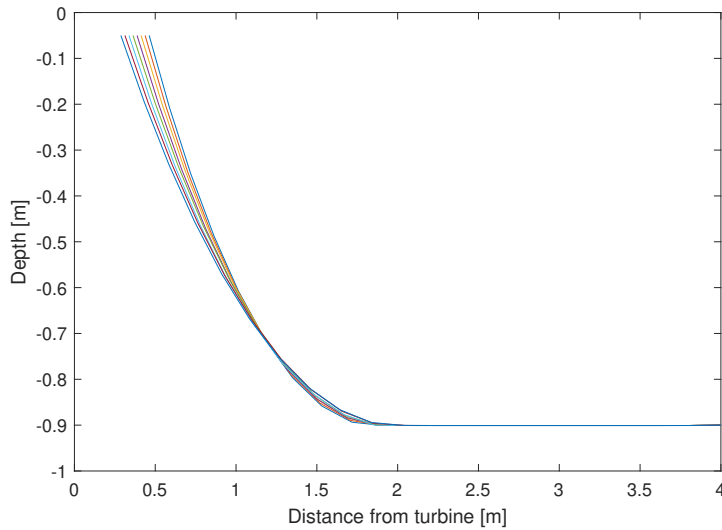


Figure 3.3: The mooring line shape over time for a small line displacement

Total excitation forcing

To determine the total force, the hydrodynamic and aerodynamic forces are combined with the mooring reactions. Since there is no aerodynamic forcing in heave, this only contains the hydrodynamic forcing and gravity:

$$\begin{bmatrix} F_1 \\ F_2 \\ F_3 \end{bmatrix} = \begin{bmatrix} F_{1,hydro} + F_{1,aero} + F_{1,moor} \\ F_{2,hydro} + F_{2,moor} - m_{tot}g \\ F_{3,hydro} + F_{3,aero} + F_{3,moor} \end{bmatrix} \quad (3.15)$$

3.2.2. Inclination angle

One of the main variables to account for is the inclination angle. The two main reasons behind are the loss of power due to the reduced frontal area of the rotor, and the operation of the nacelle at an angle they were not designed for. From the literature, a maximum inclination angle of 10 deg is acceptable[6]. Further analysis on the effect of the inclination angle on power generation is detailed in Section 5.2.

3.3. Potential theory. NEMOH

One of the considered approaches was to model the floating substructure using CAD, then mesh the submerged surfaces and finally calculate the hydrodynamic parameters using potential theory. Due to the limited budget of the project, the use of the well-known software WAMIT was discarded, and therefore an alternative had to be found. For this case the open-source code NEMOH [8] provided the capabilities needed to obtain the hydrodynamic matrices.

NEMOH resolves the flow around a submerged structure using Boundary Element Methods (BEM). The flow is assumed as inviscid, incompressible and irrotational, which allows to express the velocity as a potential. The first assumption is not always realistic, however it is challenging in the field of floating wind energy to check whether is acceptable or not, as there is lack of experimental data and high-fidelity simulations like CFD to compare the results and perform validations of the codes.

There is a series of important considerations when using NEMOH,

- only the submerged part of the structure is calculated, therefore both a hydrostatic analysis is necessary to determine the equilibrium position, and a series of matrices for the different positions the floater will experience in the unsteady motion,
- the normal vector of the panels must be oriented towards the water,
- the water-level surfaces must be removed

Figure 3.4 shows the workflow used. Firstly, the open-source tool Salome¹ is used to model the floating sub-structure. Unlike for the production phase (see Chapter 4), for this analysis simplified geometries are utilised, allowing for a balance between a realistic representation of the floater and reduced computational costs. An example can be seen in Figure 3.5b. In this case no heave plates are implemented yet, as it was used to study the effect of the central supporting column in the hydrodynamic matrices. It has been found that the contribution is relatively small, and therefore no larger efforts in modelling are needed.

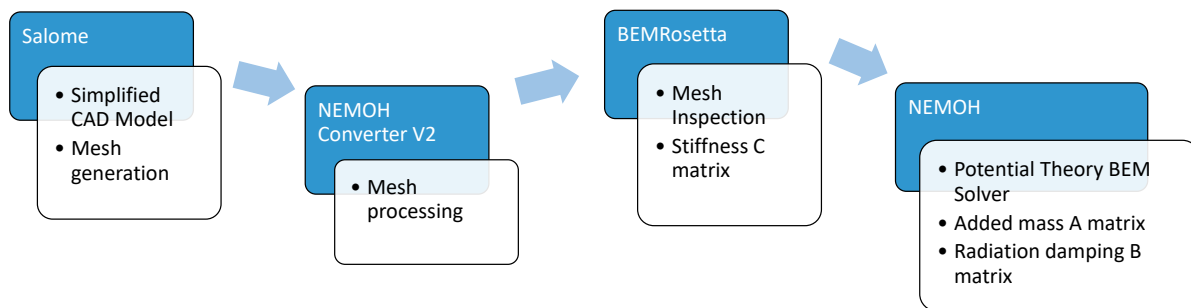
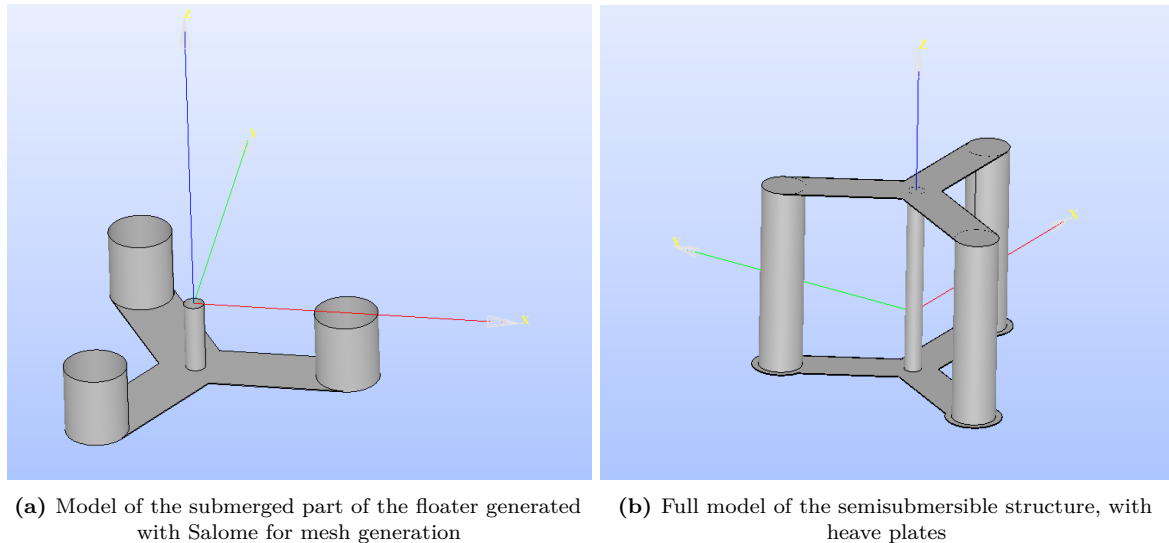


Figure 3.4: Workflow used for obtaining the hydrodynamic parameters using NEMOH

¹More information can be found <https://www.salome-platform.org/>



(a) Model of the submerged part of the floater generated with Salome for mesh generation (b) Full model of the semisubmersible structure, with heave plates

Figure 3.5: Examples of geometry modelling with Salome Geometry Module

The mesh generation can be done with Salome meshing tools. An example is shown in Figure 3.7a. As mentioned earlier, the top surfaces have to be removed. Another pitfall to avoid is that there must not be any inner face of the model, so the geometry module can be used by exploding the part and selecting the desired faces. Then the mesh module is used. The parameters are selected according to each case with the objective of a mesh with less than 4000 elements, as to reduce the computational costs, but with more than 3000 as to ensure a good resolution and accuracy. For each floater case the maximum and minimum element sizes can be given, as well as the fineness level, which is set to moderate for all cases. When the mesh in Salome is done, it can be exported into a .DAT file and continue with the mesh processing.

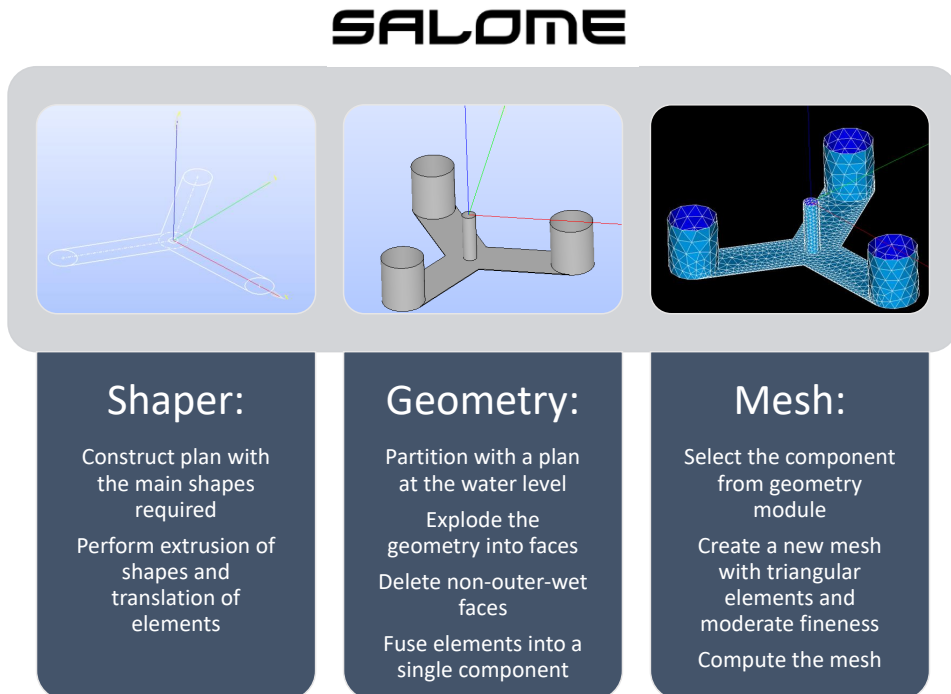


Figure 3.6: Salome workflow using shaper, geometry and mesh tools

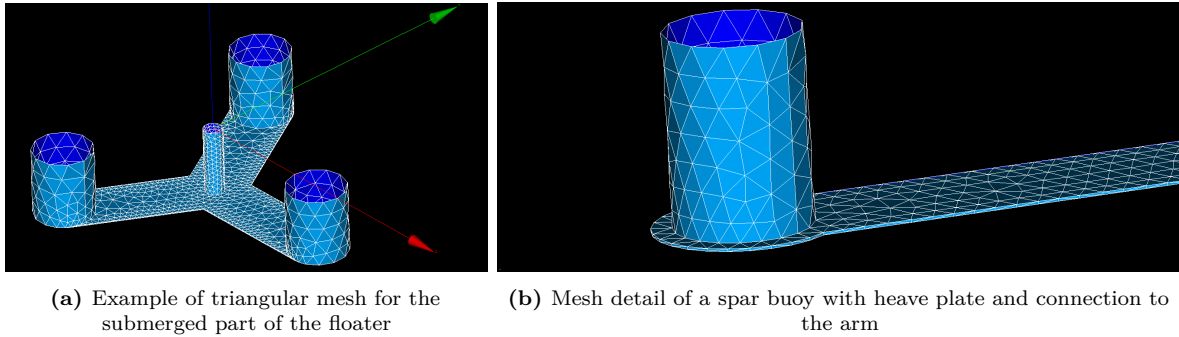
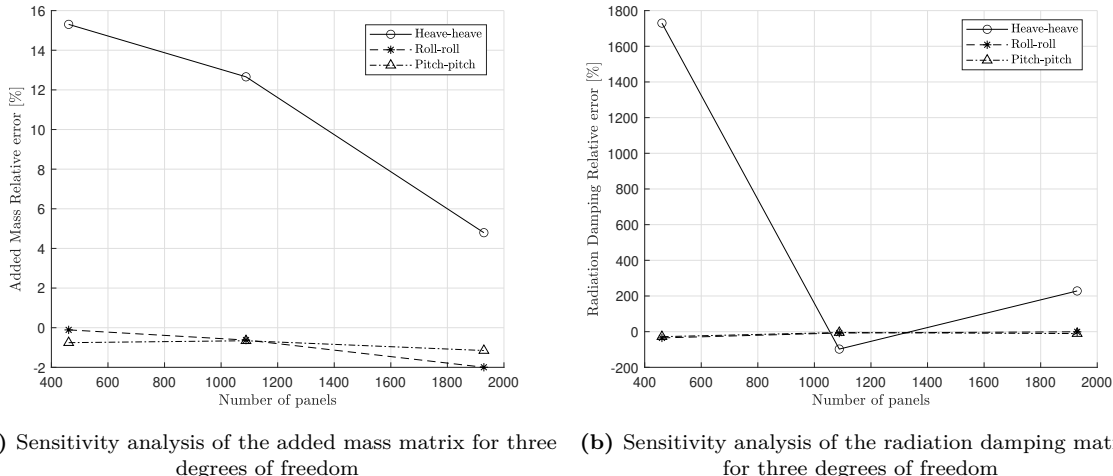


Figure 3.7: Example of Salome mesh of the submerged substructure

A mesh sensitivity analysis was performed to ensure the results are mesh-independent. Four different meshes are used, and three of them are compared to the finest mesh for calculating a relative error as

$$\varepsilon = \frac{\alpha_N - \alpha_{N=4176}}{\alpha_{N=4176}} \cdot 100 \% \quad (3.16)$$

where α_N is the value of a matrix element, and $\alpha_{N=4176}$ is the value for the most refined matrix. The calculations are done for a wave frequency of $\omega = 4.1 \text{ rads}^{-1}$. The results are shown in Figure 3.8. As seen in Figure 3.8a, the error for the heave-heave added mass decreases significantly with the number of mesh panels. On the other hand, Figure 3.8b shows an irregular behaviour of the heave-heave radiation damping, with significant errors as compared to roll-roll and pitch-pitch radiation damping. This has been reported in the consulted literature as one of the issues faced with NEMOH. This aspect requires further analysis as well as validation of the results.



(a) Sensitivity analysis of the added mass matrix for three degrees of freedom (b) Sensitivity analysis of the radiation damping matrix for three degrees of freedom

Figure 3.8: Mesh sensitivity analysis for $N = 461, 1088, 1929$ panels as compared to $N = 4176$ panels

To connect Salome with NEMOH, P. Schmitt (Queen's University Belfast) has developed an interface programme to process the mesh output from Salome and adapt it to the requirements². The simple operation consists in providing the mesh from Salome, and the `Nemoh.CAL` file where the mesh information will be updated. This code usually takes a significant time to run for large meshes.

²The software package can be found on <https://box.lheea.ec-nantes.fr/index.php/s/e1nJ0rYVK2TqWfY>

The next step is to inspect the mesh using BEM Rosetta. The main issue to look for is the orientation of the vectors normal to the faces. Additionally, the stiffness matrix is provided when loading the mesh file.

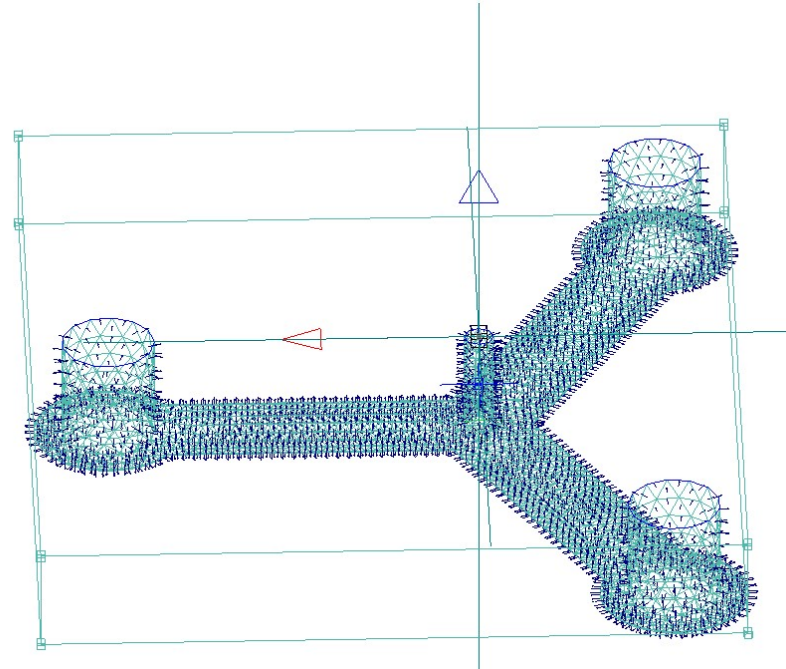


Figure 3.9: Example of BEMRosetta mesh inspection tool

Finally, NEMOH can be run with the output files from NemohConverter. The inputs needed for the main function

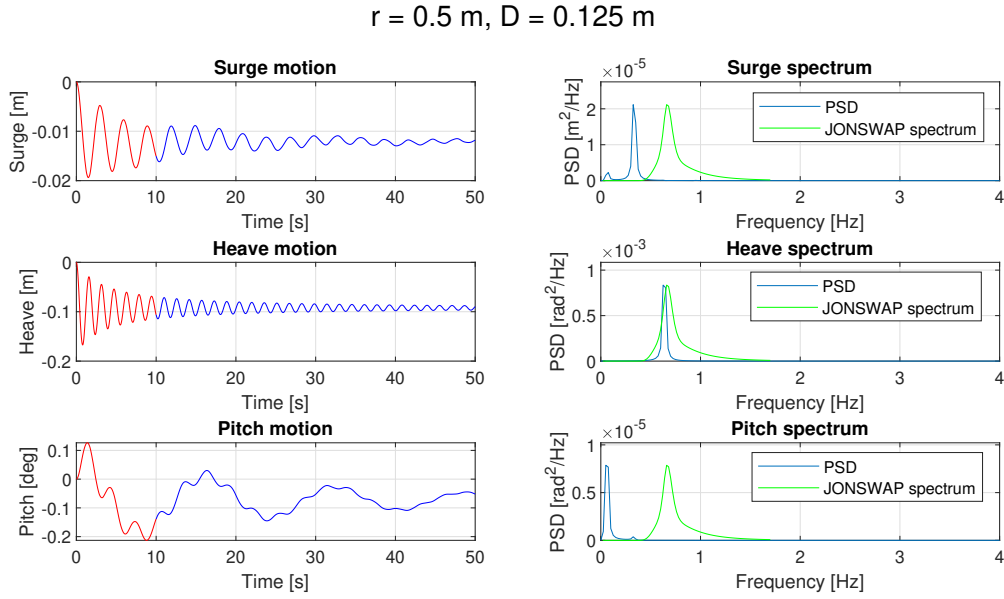
3.4. Simulation results

After all the system properties and excitation forces are known, the model can be ran. First, decay tests to obtain the natural frequencies in each degree of freedom are performed, and secondly, a full wind-wave climate simulation is done.

A comparison of the results from AxiMesh and Salome was not conducted since the results from the full model of the floater are a higher fidelity model and hence was used.

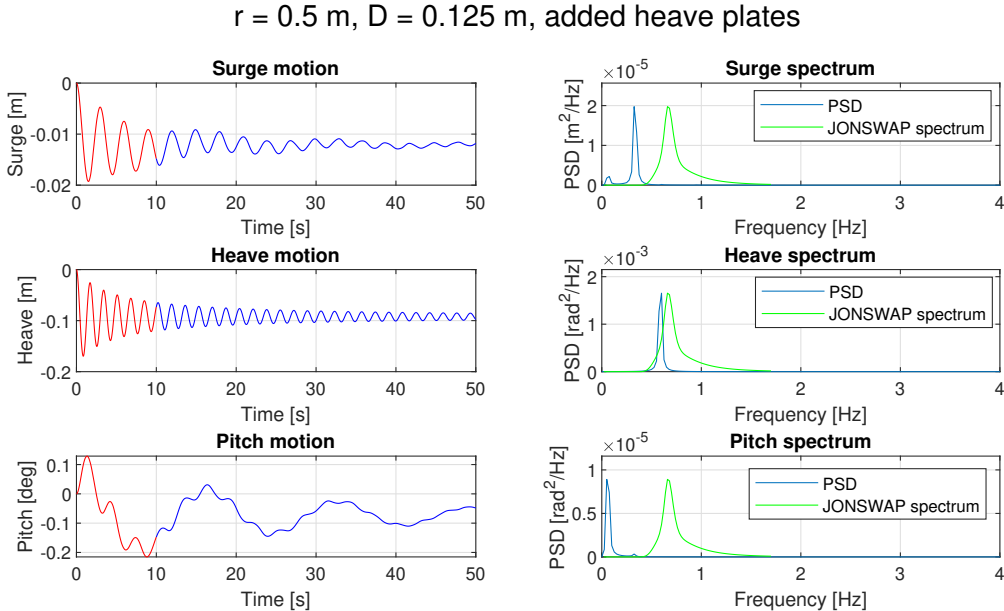
3.4.1. Natural frequency analysis

Several floater designs are processed through Nemoh to obtain the system properties. They are each analysed with the model, to see if their natural frequencies fall in the domain of the frequencies of the excitation forces. Their time domain response that is found with the model is translated to the frequency domain through a Fourier transform to see its characteristics. The blue peaks in the figures are the peaks of the system response, and the green peak is the given JONSWAP spectrum.



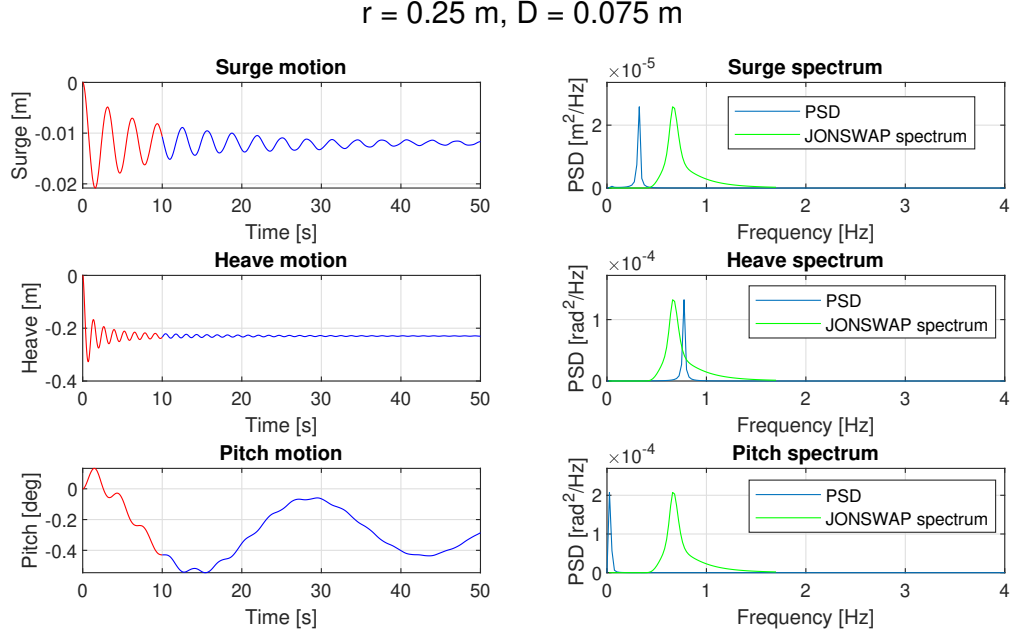
Above is a decay test of a floater with an arm length of 0.5 meter and a buoy diameter of 0.125 meter. It can be seen that especially the heave natural frequency is close to the peak frequency of the JONSWAP spectrum. The natural frequency in pitch is very low. This can be explained by the large added mass in pitch because of the floater arms that work as heave plates.

This floater design is very susceptible to resonance in heave. To prevent this, some extra heave plates are added in the below simulation:

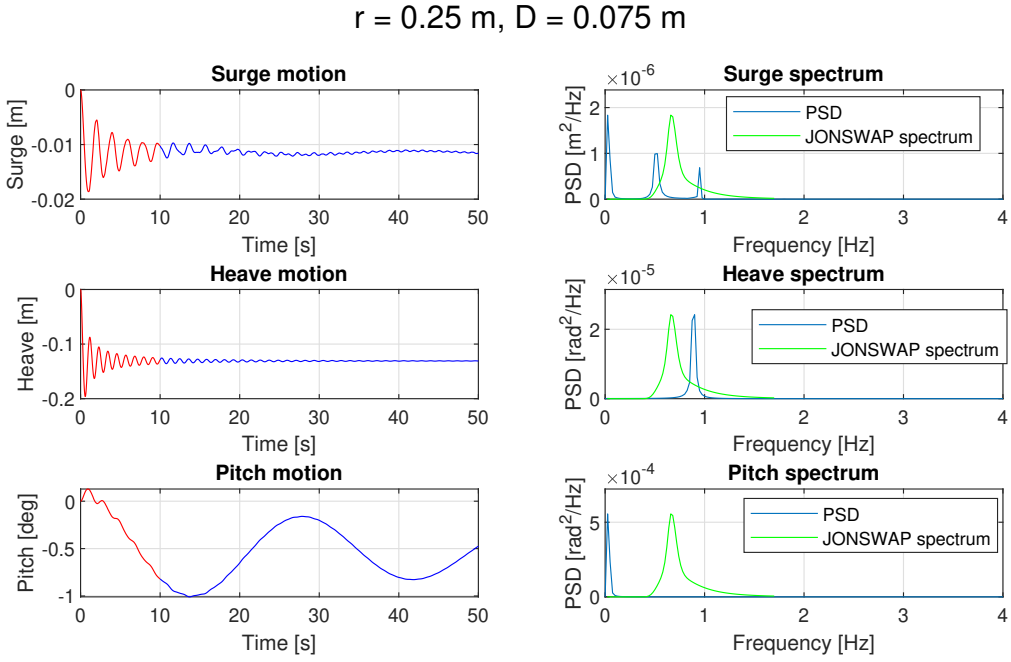


It can be seen that the natural frequency remains roughly the same, because the arms of the floater already provide a lot of damping in heave. Adding heave plates therefore does not

mitigate the problem. To see how different floater designs respond, a different arm length and buoy diameter are chosen for the following decay test:



It can be seen that the natural frequency goes up slightly. The natural frequency is determined by the ratio of stiffness over mass. The hydrostatic restoring stiffness goes down for a smaller diameter, but the added mass also decreases. These balance each other out, and result in only a slight change in natural frequency. To move the natural frequency further away from the JONSWAP peak, the mass of the floater is reduced:



It can be seen that this does shift the response away from the JONSWAP peak. It however means that the floater will be less stable in pitch. To increase this stability, the arms are made larger. To see the different designs in action and make a better comparison, full scale simulations are performed next.

3.4.2. Full simulations

To get an idea of the floater behaviour in competition environment, full simulations must be performed as well. This gives an idea of the displacement magnitudes and helps choose the design parameters of the floater. The first full scale simulation can be seen in figure 3.10. The red part indicates an initial transient response which is not taken into account for the frequency domain analysis.

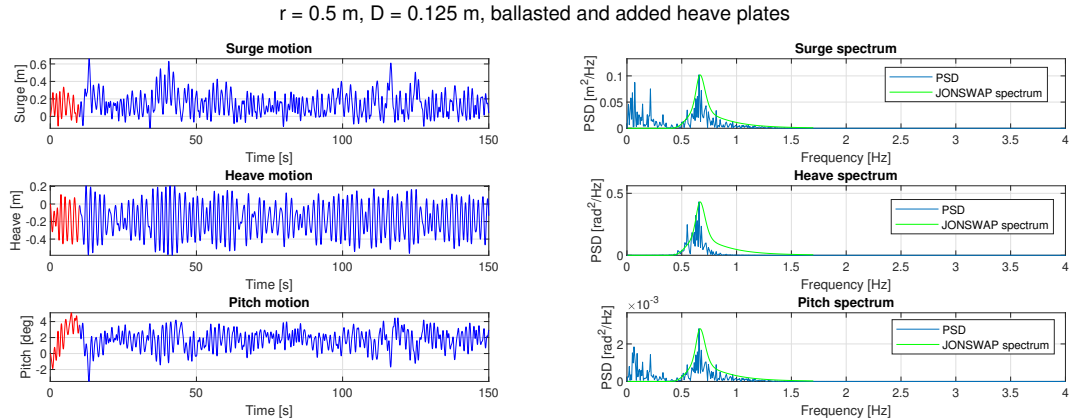


Figure 3.10: The full response to the wind wave climate of the system

All DoFs show an excitation peak under the JONSWAP spectrum. There is also some low

frequency excitation, because of the wave loads differing between the different buoy locations. It can be seen that there is a small mean displacement for the turbines pitch, but this is relatively low at around 2 degrees. The largest oscillations happen in heave. This is because the natural frequency is activated and the structure starts to resonate. With oscillations like this, the structure needs to be designed to have long buoys to avoid the top of the floater going below mean water level. A simulation of a smaller buoy diameter is also run, to see how it responds to the full wind and wave climate.

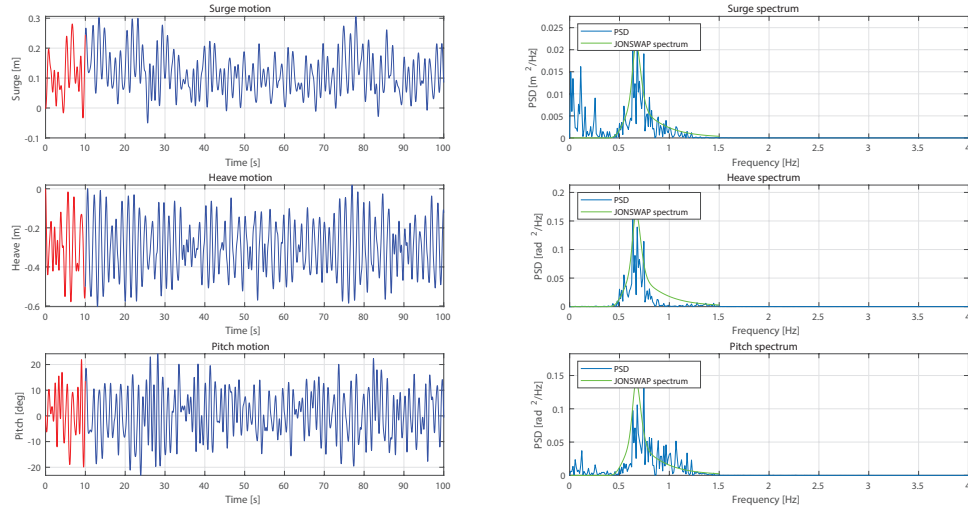


Figure 3.11: Full response to the wind wave climate of a smaller diameter buoy

It can be seen that although the floaters natural frequency is further from the JONSWAP spectrum peak, it can be seen that the smaller stability results in higher pitch displacements. The choice is made to go for a larger diameter floater to limit this large pitch angle.

3.5. Simulation challenges and pitfalls

The hydrostatic and hydrodynamic analysis of the floaters posed a large challenge, especially due to the lack of the access to software. Initially, the advice given from a professor was to use NEMOH as a replacement to WAMIT, since it is open source. However, since it is not an extended software, conventional CAD tools, such as Rhino, do not offer direct output format of the mesh to NEMOH, thus requiring a converter software, such as BEM Rosetta. After most of the simulations were performed, we came across with OpenWarp, another open source code which could have been a better option to NEMOH according to [9], for instance by removing an irregular frequency behaviour, which can be easily seen as peaks and troughs for certain frequencies of the radiation damping and added mass, plus some extra capabilities. Future work could consider using this software and compare the obtained results.

SolidWorks, Rhino and Salome were used to try and create the floater structure to process it with NEMOH, but both Rhino and SolidWorks required the BEM Rosetta interface, which is likely the result of the error. Salome's mesh .DAT output format allows the conversion of the mesh to the NEMOH interface, but the reliability of the results are difficult to analyse because of the outputs of NEMOH as various text files were not easily processed, in fact the tool BEM Rosetta offers a postprocessing tool for NEMOH outputs, which crashed when the Salome mesh were used, and not when simple NEMOH meshes were created.

Some problems were also experienced with MoorDyn. There is also not a lot of documenta-

tation available on it, and it can difficult to configure it with the correct line properties.

Modelling pitfalls with Salome

Salome offers simple tools to model structures, however some pitfalls where spotted. When using Salome shaper it is recommended to use parametric design, that is, defining the measurements as parameters which can be easily changed and would result in changes in all the shape's "children"³. This capability is largely used to quickly perform optimisation iterations.

When the geometry has been modelled in the shaper tool the faces of interest must be extracted. This is easily done using the commands *partition*, *explode* and *fuse*. The latter however may result in errors if all the faces are combined in a single step, for this reason is recommended to combine the faces slowly and wisely.

Once the geometry is ready to mesh, the meshing tools of Salome can be used. In some of the consulted documents it was stated that NEMOH can only work with quadrangular elements. This has been proven not to be the case, so it is highly recommended to use triangular mesh elements, as it leads to better cell aspect ratios, and thus convergence of the solution and less numerical errors from the current project's experience.

³Children in the CAD jargon is used to referred to dependent geometries, shapes or components that are constructed based on a previous element.

4

Production of the scaled model

From all the data and design choices in Chapter 2, a scaled model can be designed and produced. This chapter will discuss the design and material choices of the model, the bill of material, and the expected production plan.

4.1. Model Design

Through iteration of the hydrodynamic simulations from Section 3.2, a layout was found that is stable in the pitch, heave, and surge degrees of freedom. This layout consists of 3 columns of 125mm diameter PVC pipe, arranged in a triangular orientation. A fourth additional central column supports the wind turbine, this is also made of PVC but has a diameter of 40mm to reduce weight. This layout increases the water plane stability of the structure at a relatively low weight. The columns are capped off with PVC end caps, and are sealed with a water tight sealant. The columns and caps are connected to laser-cut aluminium heave plates by 3d printed brackets, which also have connection pieces for diagonal 40mm PVC cross-braces. These cross-braces should reduce the oscillation of the outlying columns by increasing the inertia. It is expected that the 3D printed parts will not be made watertight, as their internal volume is relatively low compared to the PVC pipes, and as coatings for these tend to be toxic and hard to work with. (source?) The turbine is mounted to the central column and the upper heave plates by a bracket. The bracket also connects the central column to the bottom heave plate to allow for load transfer from the turbine. All these elements are combined into the final design, which can be seen in Figure 4.1.



Figure 4.1: Final design for the floater

4.2. Bill of Materials

In this section, the elements which make up the floating platform will be discussed, and a bill of materials will be set up.

Materials have been sourced that can be acquired with relative ease at hardware stores or online. For the main structural elements, PVC pipe is used as it is designed to be watertight and as it is relatively light. It is also easy to cut to shape and glue, which is expected to make production easier.

The main elements to reduce heave will be made from aluminium sheet metal. This material is lightweight, and can be laser-cut for items of the contests scale.

To connect these elements together, 3D printed PLA-parts are used, as they can be designed to take on many different shapes and sizes. These parts are not water-tight, and take long to produce. On the other hand, they do allow for a reduction in the amount of parts that need to be glued together.

All items used for the floater are listed in Table 4.1, along with their estimated masses, dimensions, and costs in Euro. Data for PLA is based on pricing from 123-3d.nl and weight estimations from CURA. Data for the aluminium plates is based on pricing from Hornbach.nl and weight estimations from solidworks. All other elements are based on pricing from Gamma.nl and weight estimations from either Gamma.nl or Solidworks. Some data are not yet known as of the making of this report, these are marked as 'tbd'. Total values are given as well for mass, dimensions, and price, these exclude any influence from the to be determined parameters.

Table 4.1: BOM Unsinkable5 Floater

Part	Description	Qty	Unit Mass	Dimensions L x W x H	Unit Cost	Total cost
1	PVC Outboard Spar	3	496g	125x125x450	3.38	10.13
2	PVC Centre Spar	1	86g	42x42x450	0.90	0.90
3	PVC Cap 125 mm	6	tbd	129x129x30	1.49	8.94
4	PVC Cap 40 mm	2	tbd	42x42x25	0.49	0.49
5	PVC Crosstie	3	86g	42x42x450	0.90	2.70
6	Aluminium Heave Plate	6	162g	445x200x1	4.48	26.90
7	PLA Heave Plate Connector	6	92g	235x190x24	2.02	12.14
8	PLA Crosstie Connector	6	66g	55x55x100	1.45	8.71
9	PLA Turbine Connector	1	72g	130x130x55	1.53	1.53
10	PLA Centre Spar Connector	2	41g	130x130x15	0.90	1.80
11	Mooring Chain	3	tbd	tbd	tbd	tbd
12	Carabiner 8x80 mm	3	60g	80x40x8	2.99	8.97
13	Thames & Kosmos Wind Kit	1	998g	600x200x800	39.95	39.95
14	Bolt M8x60 20 piece box	1	tbd	8x8x60	12.49	12.49
15	Bolt M8x40 6 piece box	1	tbd	8x8x60	3.99	3.99
16	Bolt M6x20 12 piece box	3	tbd	6x6x20	2.99	8.97
TOTAL		4.9kg	784x784x1274		139.64	

4.3. Production Plan

In the weeks following the submission of this report, the floating platform will be designed and built. In this section, the production plan will be presented.

4.3.1. Pre-production stage

Before production starts, we intend to prototype certain solutions to see if they are feasible. Particularly with 3D printing, this is an important step to carry out, as it allows iteration before the final design. At the time of writing this report, a number of designs have been made for the brackets connecting the heave plates to the PVC pipes. Initially the idea was to clamp the aluminium plates between two flat brackets, but since the shapes are being laser cut they can be fastened by bolts, which increases reliability of the construction. The need to attach diagonal elements to increase rigidity has led to a new prototype. This is pictured in Figure 4.2.



Figure 4.2: Second iteration of the Heave Plate Connector and Crosstie Connector

There were a number of issues with the printing and support material on the second iteration. For the third iteration, the ring was made slightly smaller, and the connection bracket was made slightly shorter, allowing for fewer issues during printing, and a shorter printing time. This bracket slightly limits the angle of the diagonal bracket, but this appears to have no negative influence for the current design.

4.3.2. Production stage

Following the pre-production prototyping, the main production of the floater can be started. This phase consists of 3D printing parts, cutting pipe to scale, laser cutting aluminium plates, and assembling the parts together with bolts and glue. The production plan can be seen in Table 4.2. Details concerning testing of the model and its parts can be found in Chapter 5.

Table 4.2: Production Plan of the floater

Date	Task	Description	Parts Required	Tools Required	Est. Time (hour)
27/04	Print Prototype Heave plate connector	Print a prototype connector and bracket to connect the heave plates to outlying spars. Prototype deemed unreliable, redesigned to be more robust.	3D printer filament	3D printer	8
	Material evaluation	Materials evaluated and choices for the floater finalised	PVC pipes, chains	Scales, calipers	2
29/04	Print Prototype Heave plate connector	Print a prototype connector and bracket to connect the heave plates to outlying spars. Prototype needed changes	3D printer filament	3D printer	19
30/04	Print Prototype Heave plate connector	Print a prototype connector and bracket to connect the heave plates to outlying spars. Prototype succesful	3D printer filament	3D printer	18
01/05	Print Heave plate connector	Print a connector and bracket to connect the heave plates to outlying spars	3D printer filament	3D printer	18
02/05	Print Heave plate connector	Print a connector and bracket to connect the heave plates to outlying spars	3D printer filament	3D printer	18
03/05	Print Heave plate connector	Print a connector and bracket to connect the heave plates to outlying spars	3D printer filament	3D printer	18
04/05	Print Heave plate connector	Print a connector and bracket to connect the heave plates to outlying spars	3D printer filament	3D printer	18
	Lasercut heave plates	Lasercut the aluminium sheets to fit on top of the brackets	Aluminium sheets	Lasercutter (outsourced)	24
	Sawing PVC spars to size	Cut the PVC pipe to scale for the vertical columns	PVC pipe diameters: 125mm 44mm	Handsaw, holder/vice, marker, ruler	2
	Adhesion of caps to PVC	Glue PVC caps to the cut PVC pipes	PVC cap	Glue/epoxy	2
05/05	Print Heave plate connector	Print a connector and bracket to connect the heave plates to outlying spars	3D printer filament	3D printer	18
	Pick up lasercut materials	Pick up the lasercut materials from the day before and see how well they fit to the brackets	Lasercut aluminium	Bolts	1
06/05	Print Turbine Connector	Print a connector to connect the turbine to the heave plate	3D printer filament	3D printer	9

Date	Task	Description	Parts Required	Tools Required	Est. Time (hour)
07/05	Print Centre Spar Connector (x2)	Print 2 connectors to connect the centre spar to top and bottom heave plates	3D printer filament	3D printer	10
08/05	Sawing PVC spars to size	Cut the PVC pipe to scale for the vertical columns	PVC pipe diameters: 125mm 44mm	Handsaw, holder/vice, marker, ruler	2
	Adhesion of caps to PVC	Glue PVC caps to the cut PVC pipes	PVC cap	Glue/epoxy	2
	Test design	Test the viability of the current design a lake	Floater Turbine	Lake	2
09/05	Evaluate test performance	Evaluate the test performance and identify areas where improvement can be made	Test data		2
	Design fixes and patches for the system	Design fixes and changes to the system to improve performance	Evaluation results	CAD	4
10/05	Implement fixes	Implement any fixes (if any)			4
11/05	Test design	Test the viability of the current design a lake	Floater Turbine	Lake	2
	Design fixes and patches for the system	Design fixes and changes to the system to improve performance	Evaluation results	CAD	4
	Implement fixes	Implement any fixes (if any)			2
12/05	Implement fixes	Implement any fixes (if any)			8
13/05	Test Day	Evaluate final performance of the floater	Floater turbine	Atlantic Tank (Deltares)	4

4.4. Structural integrity

The structural integrity of the design has been iterated over a number of steps. In this section, we will discuss some of the larger design choices made during the process, and their expected impact.

Initially, the floater was designed as seen in Figure 4.3. This structure was expected to have a high structural integrity due to the thick arms, but the hydrodynamic parameters simulated were not favourable. The floater was scaled up, which gave thicker towers but thinner upper and lower plates. The PVC pipes are stiff due to their large diameters and corresponding high moments of inertia, while the aluminium heave plates are less stiff as they have a low inertia in the bending direction. To counter this reduction in structural integrity, diagonal arms were added from the bottom of each column to the top of the next, in a counter-clockwise direction. It is expected that the moment of inertia of the cross-section of each arm will increase, leading

to an expected reduction in deflection. As all arms will be directly linked, it will prevent the arms from moving freely by themselves, leading to an expected more consistent dynamic behaviour.

The expected issues with deflection and oscillation could also be reduced by replacing the top heave plate with a pipe. This however has the negative effect of making production harder for the scale model, as the pipes would need to be cut to fit perfectly, or a bracket to connect both. This would require more unique parts, requiring more engineering time. While this solution could then increase the structural integrity further, it was decided that the trade-off in production time and practicality of construction was not worth it.

4.5. Practicality of construction

The floater must be easy to produce, reproduce, and transport. This holds for both the lab-scale model designed in this report, and any eventual full-scale models. In this section, the factors that affect the lab-scale turbine's construction practicality will be discussed.

The turbine is designed to be modular, with elements such as the outlying spars, heave plates, and attachment brackets all being designed this way. This has the perk of requiring less time to prototype and test designs, but is disadvantageous if the design does not work, as all elements must be rebuilt or redesigned. To offset this, it was chosen to prototype critical elements in advance, and to choose materials that are widely available and easy to modify. Most chosen materials are easy to purchase and adapt, requiring simple modifications like sawing or gluing to be used in the final design. Additionally, most parts can be bolted together, so if some parts do not work as intended, they can easily be replaced with others.

The modularity of the floater is also useful for transport and installation. By being modular, it can be packed relatively tightly for transport. The Large 125mm PVC pipes and connection brackets are the bulkiest items, and will require more space for transport. Smaller PVC pipes are easier to transport, and have a lower mass. Wherever the structure does not require elements to contribute to hydrodynamic behaviour such as floating or damping, these pipes can be used.

Assembly at location can be made easier by pre-assembling pieces in advance, for example by attaching the 3d printed brackets to PVC tubes. Assembly by bolts means that, while there are many items that need to be bolted together, the time it takes to make a connection is lower and requires a limited amount of tools. The disadvantage of a bolted connection in salt water is corrosion, but since this floater will not be exposed to salt water for extended periods of time, this is considered acceptable.

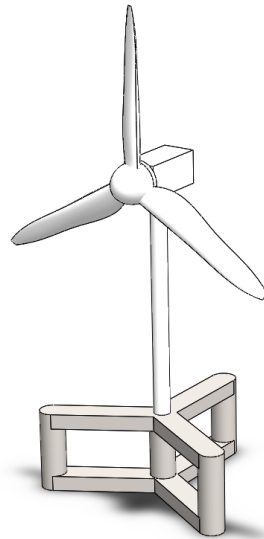


Figure 4.3: First floater design with turbine for scale

5

Testing of the model

The scaled model of the floater parts and turbine needed to be tested to validate the simulations and build the full scale semi-sub. The turbine was tested in a wind tunnel to determine the aerodynamic loads of the turbine. The 3D printed parts also needed to be tested for porosity to take into account their change in mass once submerged. Unfortunately, the full scale floater could not be built and tested in time to be added to this report.

5.1. Wind Tunnel Test

Before the testing of the floater itself, the wind turbine was tested in the Open Jet Facility at TU Delft to measure the thrust force of the turbine. A support structure, seen in Figure 5.2a was designed using SolidWorks, to hold the tower in place using the provided base supports as seen in Figure 5.1.

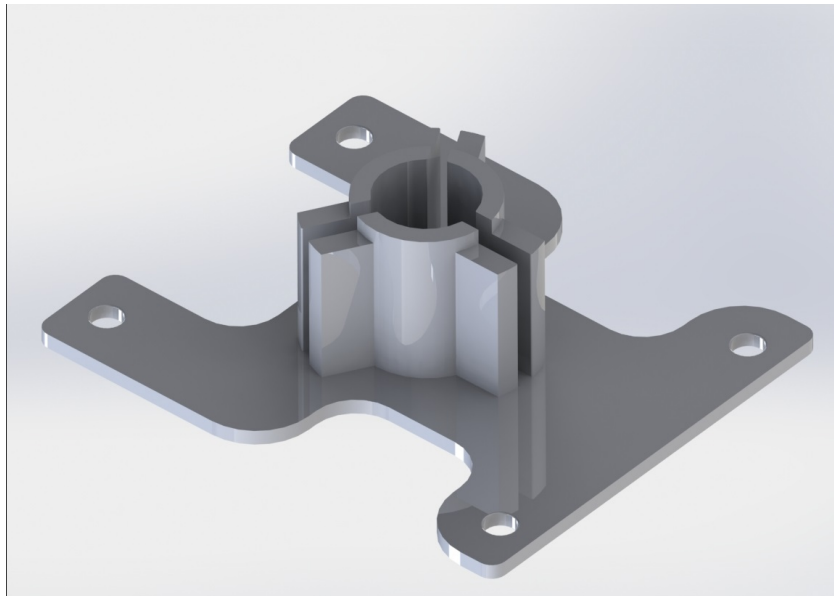
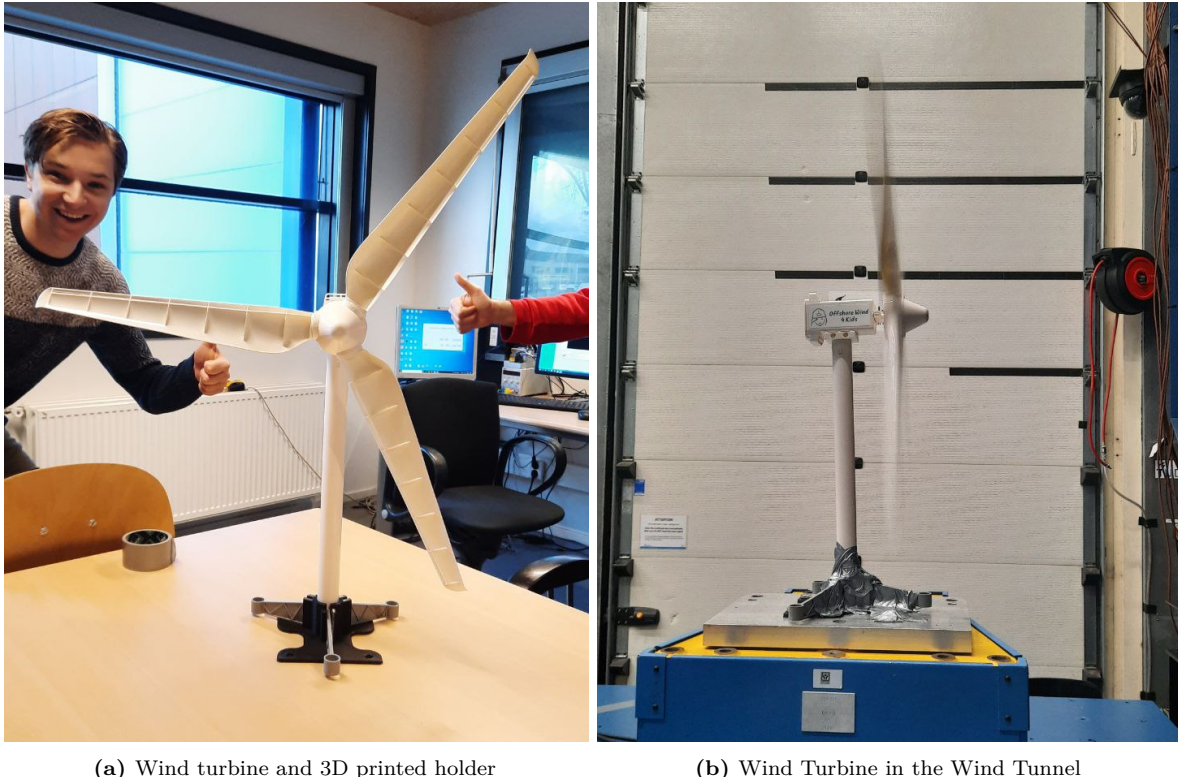


Figure 5.1: 3D Printed Holder for Turbine

The base was made to be screwed into a balance to measure the thrust force on the turbine during operation as seen in Figure 5.2b. These forces were measured for wind speeds within the Beaufort scale requirements of the contest, and the thrust coefficient, c_T , was calculated as

**Figure 5.2:** Wind tunnel set-up

$$c_T = \frac{F_x}{0.5\rho V^2 \pi R^2} \quad (5.1)$$

where F_x is the force in the wind direction, V is the wind speed and R the radius of the rotor. The thrust coefficient was calculated for each wind speed measured, the results of thrust force and c_T are shown in Figure 5.3 and Figure 5.4.

The turbine blade has 5 pitch settings, with 5 being the most pitched into the wind (pitching towards feather). Tests were done for pitch settings 5, 4, and 3, because the turbine did not start at lower pitch numbers. It can be assumed that the cut-in wind speed for the lowest pitch angles is significantly above the contest range, so they were discarded. For the pitch 3 and 4 two tests were taken.

When placed in the tunnel the bending of the tower is extremely evident as seen in Figure 5.2b, and needs to be taken into account when verifying the modelled loads on the turbine as well as when designing the support for the floater. The measured thrust force and calculated thrust coefficient was plotted against the wind speed.

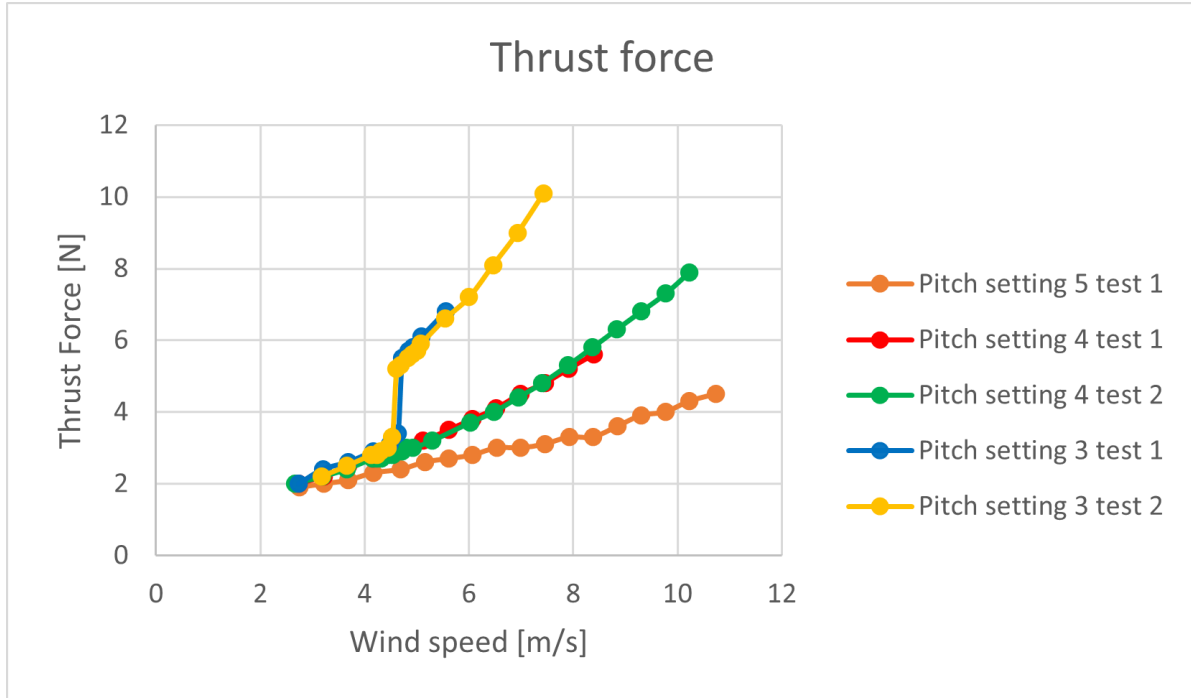


Figure 5.3: Thrust Force

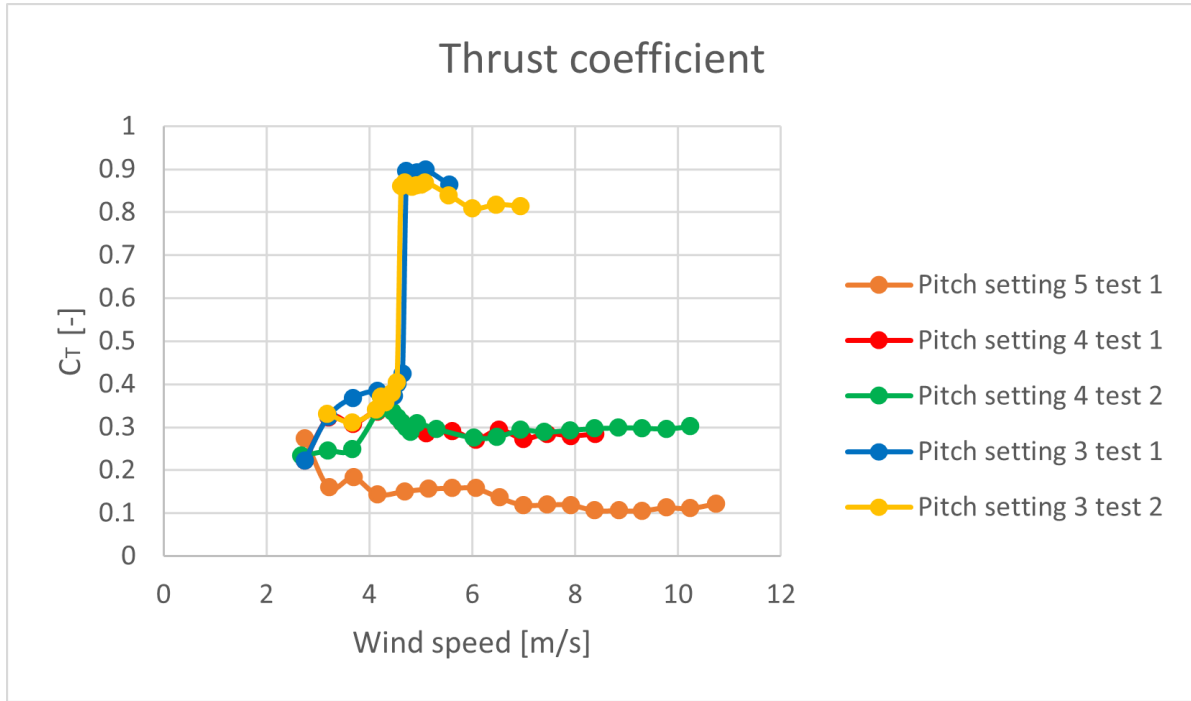


Figure 5.4: Thrust Coefficient

The thrust coefficient is the lowest for pitch 5, when the blade is pitched towards feather. The plots of the thrust force and thrust coefficient are seen in Figure 5.3 and Figure 5.4 respectively. Firstly, we notice that as we pitch towards stall, the thrust force increases with increasing wind speed. However, at a pitch setting of 3, we see that at a wind speed of around 4.6-4.7 m/s, there is a significant increase in the thrust force. At the time of the experiment,

at this velocity there was also a sudden increase in the pitch of the sound from the turbine, that was coupled with a sudden increase in the rotational velocity as well. The aeroacoustics and rotational velocity were not measured and hence, this data is not be provided here. This is most likely because the turbine is stalling. Furthermore, when the turbine was pushed to higher velocities at this pitch setting, the rotational speed was too high and the plastic shaft melted and broke. This was at a wind speed of 7.43 m/s, which is within the recommended operational range specified by the manufacturers, which suggests that some lubrication would be needed for longer operating times. This velocity is also within the range of the challenge wind speeds.

The thrust force can be seen as a representation of the pressure difference before and after the rotor disk, and is the foundation for many models such as some actuator disk models for a wind turbine. Therefore, it can be extrapolated that more energy is extracted from the flow and hence, there is a higher power yield at this setting. However, due to the safety issues of running the turbine at a setting of pitch 3 at a velocity of 8 m/s with the additional effects of wave loads and the movement of the floater, it was decided that the blades will be pitched to setting 4, to maximise the power yield while minimising the safety risks due to high loading.

It is worth noting that the system is also unsteady and hence, as the turbine pitches due to the wave loads, there will be a hysteresis loop that will affect the aerodynamic loads, which will once again affect the pitch of the floater, creating a feedback loop. This would need to be further studied through a high fidelity unsteady model, to ensure that the unsteady loads motions of the floater are damped out and not affected by the unsteady aerodynamic loads.

5.2. Power generation efficiency

Due to the interaction of the dynamic wind and wave loads, the turbine will not be able to operate at its optimal condition the whole time and hence, there will be efficiency losses.

For onshore and bottom fixed turbines, there is some movement of the tower due to the loads, but the structure itself is fixed, and the inclination angle of the free stream wind relative to the rotor does not vary much. However, floaters add an additional six degrees of freedom to the system. In the case of this challenge, the incoming wind and waves are unidirectional and perpendicular to the rotor plane and hence, heave, surge, and pitch will be the dominant degrees of freedom.

Ideally, the goal would be to reduce the thrust on the turbine so that the rotor plane is at a lower inclination angle and hence, can harvest more power as it is perpendicular to the incoming flow. However, the angle now depends on the floater movements that arise from wave loads and their coupling with the aerodynamic loads. The wave loads will cause heaving, surging and pitching motions, which will cause the floater and turbine to move in these degrees of freedom. The combination of these motions, especially the pitching motion, will change the direction of the incoming wind relative to the rotor plane and hence affect the incoming flow velocity as well as the loads on the turbine, making them uneven. These uneven loading conditions, combined with the uneven thrust forces due to unsteady wind conditions, will increase the loads in the turbine and hence, once again affect the motions in the various degrees of freedom, making the system even more unsteady, as mentioned earlier.

Furthermore correct pitch setting of the turbine is also extremely important to optimise the power generation efficiency, but this is not as simple for the case of a floating turbine. For fixed turbines, the pitch angle of the blade would determine the angle of attack, assuming a fixed twist angle. This will affect the airfoil lift and drag forces and hence, the thrust force, which in turn affects the inclination angle and power harvested.

Figure 5.5 shows how an increase in the pitch angle (pitching away from the wind direction) increases the angle of attack and hence there will be an increase in the loads. However, this

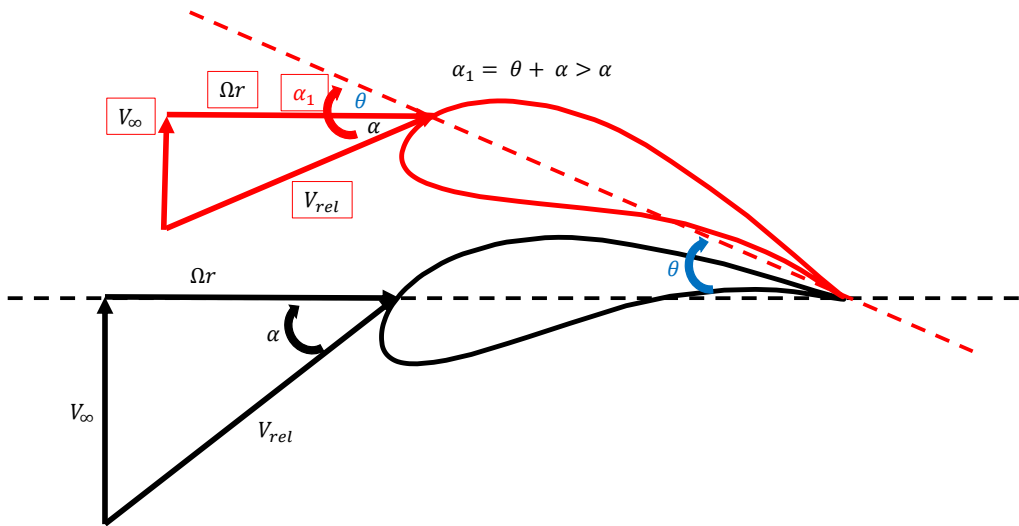


Figure 5.5: Diagram of Velocity Triangles with Change in Pitch Angle. The black line is for a 0 pitch angle and the red line indicates the new chord line when the blade is pitched by an angle θ .

also depends on the position on the $c_l - \alpha$ curve you are at. Ideally, we want to stay away from the peak in this curve to avoid stall so that the loads are not high and hence, do not affect the dynamic loads on the floater greatly. However, to avoid stall, the angle of attack should be reduced and this will in turn also lower the power harvested. Furthermore, the unsteady motions of the floater make it harder to judge the point of stall because the added pitch angle of the entire floating structure on top of the pitch of the blade can increase the resultant angle of attack on the blade and push the turbine into stall conditions, which once again increases the loads and created a feedback cycle. This is not the case for fixed turbines, because this additional pitch of the structure is not there and hence, the balance between optimising the pitch angle and the loads for maximum power yield is valid. The coupling of the wind and wave loads make this assumption no longer valid and hence, it is much harder to optimise the pitch angle for maximum efficiency.

Further studies should include an integral optimisation of the floater and rotor dynamics. However it is out of the scope of this project.

5.3. Water Test of Model

Limited water tests have been carried out as of the writing of this report. The 3D printed brackets have been tested for water absorption by leaving them in a sink overnight. After 11 hours, the brackets were weighed again. The prints were made with PLA at 20% infill. The data can be found in Table 5.1.

Table 5.1: 3D printed parts before and after immersion in water

	Heave Plate Connector	Crosstie Connector
Weight before (g)	93	46
Weight after (g)	99	55

From the table it appears that the water absorption over the course of 11 hours is not large. The Heave Plate Connector weighed 6% more, and the Crosstie Connector weighed 20% more. The structures still remained buoyant after the test, and the overall weight gain is expected to have no adverse effect on the floater's performance. An explanation for the difference in water

absorption is due to geometry. The Crosstie Connector has a larger interior volume of infill material, while the Heave-plate connector has smaller areas of infill material. It is expected that water leaking in through imperfections in the print surface can therefore penetrate easier in the crosstie connector, leading to a relatively higher weight.

Unfortunately, this version of the report does not contain the details of the water tests of the model due to the lack of access to test facilities and incomplete manufacturing of the floater due to certain time and material constraints. Final tests of the floater will be included in an updated version of the report for future reference and archiving purposes.

6

Scalability for further production

The turbine has been designed to be tested and produced on lab scale, but the performance of the turbine can also be considered if it is scaled up to full-scale. A number of design and production choices made in Chapter 2 will also likely not hold for the larger model, or may be significantly more difficult to produce. These too will be discussed in this section.

If the turbine supplied by OffshoreWind4Kids is scaled up by 200 times, the hub height would be around 80 metres, and the rotor diameter would be around 120 metres. An example of a turbine that approximates this scale is the NREL 5MW turbine, which has a hub height of 87 metres and a rotor diameter of 128 metres [10]. This will be the design scale optimised for, but according to Borg et. al. [11] floating wind will need to be designed for 15MW+ wind turbines, expected to become commonplace towards the end of the 2020s.

As stated by Borg et. al. [11], several challenges must be considered until reaching a commercially mature state. One of the problems mentioned is related to the manual fabrication and assembly of structures, which delays the deployment time horizon, heavily affected by the weather windows specially far off the coast. Furthermore, wind turbines are rapidly growing in size, thus floating structures should be able to accommodate the coming concepts.

The operation and maintenance is also an added difficulty compared to existing offshore solutions, as the continuous motion of the system poses a challenge.

6.1. Design & Production Choices For a Full-Scale Floater

It is expected when the model is scaled up the aero- and hydrodynamic behaviour will be affected significantly. As a result, certain choices made for the lab-scale model will likely no longer be viable. The scaling should take into account the non-dimensional parameters influencing the performance of the system, such as the Reynolds number, Mach number, tip-speed ratio (λ), etc. First of all the material choices can be taken into account.

PVC pipes will no longer be a suitable spar, as production at such a scale would require specialised equipment, and as it is likely not capable of sustaining the high loads applied. As stress scales with the area, a much higher area would be required, leading to either large spar diameters, or thick spar walls. The replacement for PVC pipes will likely be sheet steel, or concrete caissons for larger models. Steel has the advantage of being strong and weldable, but it does tend to corrode. Concrete spars have the benefit of being able to be produced with fewer tools, but will likely weigh more than steel spars, requiring a bigger spar to be made. This has negative consequences for transport, as the floater will need bigger equipment to be launched, assembled, and brought out to sea. Additionally, concrete cannot be recycled as compared to steel, therefore accounting must be made for the landfill footprint. The ideal

material depends on the deployment location, considering the turbine is to be tested in the Atlantic Basin at Deltares, it is expected it could be deployed in the North Sea. Since the region around the North Sea is industrialised and has generally good infrastructure, steel is a viable material for the scaled-up floater.

The Heave plates will have to be rebuilt as well. Laser cutting is not a practical option for large plates. Aluminium is relatively expensive in large quantities, and can cause galvanic corrosion in salt water. The geometry of the plates will also need to be adjusted, as the large, thin heave plates may suffer from aeroelastic instability in high wind loads. In the lab-scale model, the heave plates are likely within the boundary layer, and the upstream wind speed is lower, meaning this is a viable option. Replacing these with steel tubing is an option, although heave plates will still be required on the bottom of the floater. These can be made of sheet steel as well, or if the structure is made of concrete, these can be added to the columns when pouring.

The 3D printed brackets must also be replaced, as the material and production methods are not suitable for large scale. If steel is used for all elements, welding is an option, but this makes disassembly for maintenance or decommission much harder. Bolted connections suffer from significant corrosion in salt water environments, but do make disassembly easier. By coating and maintaining the connections properly, bolt connections can be a viable option for the floater.

The spars will need to be checked for individual oscillation under load, and if this could lead to fatigue, diagonal cross ties could be added. It is however expected that changing from heave plates to cylinders will increase the structural rigidity sufficiently to allow for the removal of the cross ties.

From all these design decisions, the final floater could look something like Figure 6.1. The floater is relatively smaller compared to the turbine, and will have relatively smaller heave plates. Connections are bolted as much as possible, and the structure is made primarily from steel. The exterior will be painted and treated to delay corrosion. All these factors should allow the upscaled floater to have similar structural integrity, with a minimised impact on production, transportation, and operation.

6.2. Cost Efficiency At Full-Scale

In this section an estimation will be made for material and fabrication costs for the full-scale floater. The scale model is made cost efficient by choosing materials and production techniques that are easy to source. On a full-scale floater a large emphasis is placed on cost and lifetime, where fatigue loads are an issue. In Section 6.1 material choice was already touched upon, and the North Sea was determined as a likely location for the turbine.

According to Borg et. al [11], there are three ways to increase cost efficiency of floating platforms. A significant cost for floating wind platforms is storage for the time during construction in port. Producing floaters on a larger scale at a quicker speed reduces the need for long term part storage, leading to an increase in costs. This would require a robust logistics system to prevent production delays. Reducing the need for specialised vessels is also a great



Figure 6.1: Example of scaled up turbine and floater system

option to become more cost efficient, as it becomes possible to charter local companies with non-specialised vessels, such as tug boats, at a lower cost. Finally, components would need to be produced on an industrial scale, like a production line. This would decrease costs due to volume production.

Materials that area considered for the floaters use case area concrete and steel. Choisnet et. al. [12] have determined data to estimate pricing for both materials. They state that steel floating wind structures cost around 4000€ per ton of steel used, and for concrete the cost is 1300€ per cubic metre. They also note that steel prices tend to fluctuate a lot, making pricing estimations variable. In their report they state that a 6MW turbine would cost about half as much to produce with concrete as it would with steel in Europe, although the roles may be reversed if steel prices are cheaper, or if aggregates for concrete aren't as readily available.

Choisnet et. al. [12] also state interesting calculations on carbon dioxide output as a result of the production proces. Their data states that for steel, the carbon emissions lie between 7018 kg/ton and 2420 kg/ton, with more recycled material reducing the carbon cost. Their data states that for concrete, the emissions are between 3376 kg/ton and 1468 kg/ton, once again depending on how much recycled content is used. Concrete is therefore a better choice from a financial and an environmental perspective, though ideally we could use one concrete floater for more than one wind turbine life cycle.

7

Conclusion

A lab-scale floating wind platform has been designed for a challenge set by OffshoreWind4Kids and Deltires. Hydrodynamic simulation, Wind tunnel testing, and Mooring Analyses have contributed to the current design. By scaling up the structure, a life-scale floating wind platform emerges that can offer opportunities for deep-sea wind farms.

7.1. Future Improvements

During the project, a number of improvements could be identified that couldn't be integrated into the current design process, but which could prove useful to future endeavours. First, the recommendation is to use OpenWarp and Salome for calculating hydrodynamic coefficients instead of NEMOH or BEM Rosetta software. This is due to extensive issues with the meshing of models if done via BEM Rosetta, and a lack of documentation on NEMOH. If funding is not an issue, a WAMIT license is also a solution. A second improvement could be to reduce the reliance on 3D-printed parts. While it is a versatile production method, it has led to production issues. Thirdly, the equations of motion based on Morisons equations, and they are linearised, while in reality the system is non-linear. To account for non-linear wave loads far from the coast and unsteady aerodynamics, a non-linear simulation should be used in future calculations. Finally, although the project timeline officially started in September, our group only started the projected in January due to academic work and a larger group splitting up and many students dropping out of the competition. Ideally, with more time, we would be able to obtain better results, but it is a point of improvement to develop as a group.

7.2. Acknowledgements

We have learned a lot throughout the course of this project and we could not have done so without the help of many people who have gone out of their way to provide us with the knowledge and skills needed to develop a floater. From Denmark Technical University (DTU), we would like to thank Assistant Professor Antonio Pegalajar-Jurado and Assistant Professor Fabio Pierella for their guidance, supervision, intuition, and support from the start. From the Technical University of Delft (TU Delft), we would like to thank Dr. Ir. Axelle Viré and Dr. Ir. Pim van der Male, and from Norwegian University of Science and Technology (NTNU) Professor Zhen Gao for their advice and support on the design and implementation. We would also like to thank Dr Mustafa Vardaroglu for sending us sources and helping answer questions. Lastly, we want to thank Deltires and OffshoreWind4Kids for organising and hosting this challenge, and for giving us this opportunity.

References

- [1] Hannah Ritchie, Max Roser, and Pablo Rosado. “CO₂ and Greenhouse Gas Emissions”. In: *Our World in Data* (May 2020). URL: <https://ourworldindata.org/co2-and-other-greenhouse-gas-emissions> (visited on 05/01/2022).
- [2] *IPCC, 2019: Climate Change and Land: an IPCC special report on climate change, desertification, land degradation, sustainable land management, food security, and greenhouse gas fluxes in terrestrial ecosystems.* Tech. rep.
- [3] Manish Karkera & Guy Griffiths (Institute for Environmental Analytics). *Show Your Stripes*. en. URL: <https://showyourstripes.info/c/globe> (visited on 05/01/2022).
- [4] *Global Energy Review: CO₂ Emissions in 2021 – Analysis.* en-GB. 2021. URL: <https://www.iea.org/reports/global-energy-review-co2-emissions-in-2021-2> (visited on 05/01/2022).
- [5] Internationale Agentur f??r Erneuerbare Energien. *Global renewables outlook energy transformation 2050*. English. OCLC: 1312334535. 2020. ISBN: 978-92-9260-238-3. URL: https://www.irena.org/-/media/Files/IRENA/Agency/Publication/2020/Apr/IRENA_Global_Renewables_Outlook_2020.pdf (visited on 05/01/2022).
- [6] Chong Ng and Li Ran. *Offshore wind farms: technologies, design and operation.* eng. Woodhead Publishing Series in Energy 92. Amsterdam [u.a.]: Elsevier WP Woodhead Publishing, 2016. ISBN: 978-0-08-100779-2.
- [7] Madjid Karimirad and Torgeir Moan. “Feasibility of the Application of a Spar-type Wind Turbine at a Moderate Water Depth”. In: *Energy Procedia* 24 (2012), pp. 340–350. ISSN: 1876-6102. DOI: <https://doi.org/10.1016/j.egypro.2012.06.117>. URL: <https://www.sciencedirect.com/science/article/pii/S1876610212011575>.
- [8] A. Babarit and Delhommeau, G. *Theoretical and numerical aspects of the open source BEM solver NEMOH*. en. Tech. rep. Nantes, France, 2015.
- [9] E. Faraggiana et al. “Computational modelling and experimental tank testing of the multi float WaveSub under regular wave forcing”. en. In: *Renewable Energy* 152 (June 2020), pp. 892–909. ISSN: 09601481. DOI: [10.1016/j.renene.2019.12.146](https://doi.org/10.1016/j.renene.2019.12.146). URL: <https://linkinghub.elsevier.com/retrieve/pii/S0960148119320257> (visited on 05/01/2022).
- [10] Jason Jonkman et al. *Definition of a 5-MW reference wind turbine for offshore system development.* Tech. rep. National Renewable Energy Lab.(NREL), Golden, CO (United States), 2009.
- [11] Michael Borg et al. “Technical Definition of the TetraSpar Demonstrator Floating Wind Turbine Foundation”. en. In: *Energies* 13.18 (Sept. 2020), p. 4911. ISSN: 1996-1073. DOI: [10.3390/en13184911](https://doi.org/10.3390/en13184911). URL: <https://www.mdpi.com/1996-1073/13/18/4911> (visited on 05/01/2022).
- [12] Thomas Choisnet, Bruno Geschier, and Geoffroy Vetrano. “Initial Comparison of Concrete and Steel Hulls in the Case of IDEOL’s Square Ring Floating Substructure”. In: Tokyo: Ideol S.A., Nov. 2016, p. 4.